



Thomas Zeiringer, BSc

# **Advanced Control Concepts for Wire Arc Additive Manufacturing**

## **Master's Thesis**

to achieve the university degree of  
Master of Science

Master's degree programme: Electrical Engineering

submitted to  
**Graz University of Technology**

Supervisor  
Univ.-Prof. Dipl.-Ing. Dr.techn. Martin Horn  
Institute of Automation and Control

Co-Supervisor  
Assoc.Prof. Dipl.-Ing. Dr.techn. NorbertENZINGER  
Institute of Materials Science, Joining and Forming

Graz, October 2021

This document is set in Palatino, compiled with [pdfL<sup>A</sup>T<sub>E</sub>X2e](#) and [Biber](#).

The L<sup>A</sup>T<sub>E</sub>X template from Karl Voit is based on [KOMA script](#) and can be found online: <https://github.com/novoid/LaTeX-KOMA-template>

---

## Affidavit

I declare that I have authored this thesis independently, that I have not used other than the declared sources/resources, and that I have explicitly indicated all material which has been quoted either literally or by content from the sources used. The text document uploaded to TUGRAZonline is identical to the present master's thesis.

---

Date

---

Signature



# Abstract

Wire Arc Additive Manufacturing (WAAM) is a promising technique for producing near-net shaped parts. Not only is the deposition rate higher than for other metal additive manufacturing techniques but also the buy-to-fly ratio can be improved. Among the challenges of this process is the dependency of the layer geometries on many variables which can lead to a distorted or curved top surface. Building high structures without a proper technique to control the geometry of the weld bead is impossible. A model of the layer height w.r.t. the travel speed is proposed based on simple considerations on the geometry. The model only requires the measurement of the layer height after each pass in contrast to most other approaches. Two controllers are suggested where one of the model parameters is assumed to be unknown and slowly varying – one observer based and one disturbance observer based approach. The model and the controllers are validated in experiments. Further more, an experiment to analyse the behaviour of the temperature field relative to the weld pool is conducted.



# Acknowledgement

This work was done at the Institute of Automation and Control. I would like to thank the Institute of Materials Science, Joining and Forming for the contribution in kind, especially Norbert Enzinger, Kurt Kerschbaumer, Leander Herbitschek and Florian Pixner for the use of the welding facility, the support with technical questions and for the execution of the welding experiments.

Special thank you goes to my supervisor Martin Horn, who supported me not only during my master thesis but throughout my studies. He was already my supervisor for the bachelor's thesis.

I would also like to thank my family for the support. Their serenity and that i can rely on them in any matter made it possible for me to complete my studies in such a stress-free manner.





# Contents

<b>Abstract</b>	<b>v</b>
<b>1 Introduction</b>	<b>1</b>
<b>2 Literature Review</b>	<b>5</b>
2.1 Welding Technologies . . . . .	5
2.2 Materials . . . . .	7
2.3 Challenges . . . . .	8
2.3.1 Process control challenges . . . . .	9
2.3.2 Material related challenges . . . . .	10
2.4 Ancillary Processes . . . . .	12
<b>3 Problem</b>	<b>17</b>
3.1 Significant quantities . . . . .	17
3.2 Accessible quantities . . . . .	23
3.3 Problem statement . . . . .	23
<b>4 Solution</b>	<b>25</b>
4.1 Model . . . . .	25
4.2 Controller design . . . . .	28
4.3 Observer error based controller . . . . .	30
4.3.1 Stability . . . . .	32
4.3.2 Discussion . . . . .	33

## Contents

---

4.3.3	Implementation . . . . .	33
4.4	Disturbance Observer Based Controller . . . . .	35
4.4.1	Further derivation . . . . .	35
4.4.2	State controller . . . . .	36
4.4.3	Stability . . . . .	36
4.4.4	Summary . . . . .	37
4.4.5	Implementation . . . . .	37
<b>5</b>	<b>Experiments</b>	<b>39</b>
5.1	Laboratory Setup . . . . .	39
5.2	Measurement of the layer heights . . . . .	40
5.3	Data Logging . . . . .	41
5.4	Parameter Study . . . . .	42
5.5	Unidirectional Single Bead Multi Layer Experiment . . . . .	46
5.5.1	Uncontrolled unidirectional single bead multi layer experiment . . . . .	50
5.6	Bidirectional Single Bead Multi Layer Experiment . . . . .	53
5.6.1	Uncontrolled bidirectional single bead multi layer experiment . . . . .	56
5.7	Temperature Field during the welding process . . . . .	58
<b>6</b>	<b>Conclusion</b>	<b>63</b>
6.1	Review of the Content . . . . .	63
6.2	Discussion of the results . . . . .	64
6.2.1	Layer Height w.r.t. travel speed . . . . .	64
6.2.2	Heat input . . . . .	66
6.2.3	Delay in $\frac{w}{v}$ . . . . .	67
6.3	Discussion of the Controllers . . . . .	67
<b>7</b>	<b>Outlook</b>	<b>69</b>
	<b>Bibliography</b>	<b>73</b>

# List of Figures

2.1	Classifications of Directed Energy Deposition processes according to Dass and Moridi, 2019 . . . . .	5
3.1	Gas Metal Arc Welding (GMAW) and its quantities. $w$ . . . Wire feed speed. $v$ . . . Travel speed. $z [n, k]$ . . . height of layer number $n$ at position number $k$ . . . . .	17
3.2	The volume flow $\dot{V}_w$ into the volume $\Omega$ must be same as the volume flow $\dot{V}_v$ out of it – otherwise material would accumulate. . . . .	19
4.1	The control action will be delayed due to the finite dimensions of the weld pool. Only after one full length of the weld pool, it can be assumed that the control action took full effect. However, we can estimate the delay in the model by half the length of the maximal delay $p_{max}$ which means the control action is halfway executed. . . . .	27
5.1	Two layers for each of the 5 different tested travel speeds. One trial was redone, therefore there are six beads. . . . .	43

5.2	The layer height over the position for different travel speeds. The welding direction is towards positive numbers of the position $k$ . There is a significant bulk at the start and scallop at the end. The dashed lines are linear approximations for each position. The slope of the lines is very uniform for the lines in the centre, which indicates that the model (3.5) could work well. . . . .	44
5.3	The layer heights are averaged over the weld direction around the centre for each travel speed. Also the approximation of $f(v)$ using equation (4.15) and (4.2) is shown as the solid blue line. A good match of the model and the measurement data can be observed. . . . .	45
5.4	Single bead multi layer experiment with the controller from section 4.3. The cubes show the added height for each segment and layer. The colour indicates the travel speed $v[n, k]$ . . . . .	46
5.5	Result of the controlled single bead multi layer experiment. For details on the geometry see figure 5.4 . . . . .	47
5.6	Layer height $\Delta z$ w.r.t. the travel speed $v$ and the layer $n$ . Each line consists of all the measured data points (except the first and last 3 segments) for one layer. The gray surface is the model from equation (4.2). The vertical dashed lines indicate the difference to the model. Note: each point in the plot corresponds to one single measurement during the experiment. If there are multiple points at the same $(v, n)$ location, the travel speed was measured multiple times at the same layer and yielded different results in the layer height. . . . .	48

5.7	Uncontrolled single bead multi layer experiment with a constant travel speed of $v = 10 \frac{\text{mm}}{\text{s}}$ (foreground) in comparison with the controlled single bead multi layer experiment (background). The data in the upper section was not recorded, therefore the layer borders are missing at the upper layers. . . . .	51
5.8	Result of the uncontrolled single bead multi layer experiment. . . . .	52
5.9	Single bead multi layer experiment with the controller from section 4.4 with alternating weld direction (equation (4.21)). The cubes show the added height for each segment and layer. The colour indicates the travel speed $v[n, k]$ . . . . .	54
5.10	Results of the controlled (middle) and uncontrolled (foreground) single bead multi layer experiment with alternating weld direction. The small wall in the background is a test run for the desired layer height $\Delta z$ . . . . .	55
5.11	Uncontrolled bidirectional single bead multi layer experiment with a constant travel speed of $v = 14 \frac{\text{mm}}{\text{s}}$ (background) in comparison with the controlled bidirectional single bead multi layer experiment (foreground). . . . .	56
5.12	Preparation of the specimen for the temperature field experiment. . . . .	58
5.13	Temperature over time for both passes of the temperature field experiment. The red surface is the position of the weld gun over time. The black curve is the temperature below the weld gun. The data is also shown as a 2D-plot in figure 5.14. . . . .	59
5.14	Temperature below the weld gun over the length of the specimen. Keep in mind that the measurements were not taken at the same instance of time but only when the weld gun was above the measurement point. . . . .	60

5.15	Temperature relative to the weld pool. A relative position $\sigma = 20$ mm means that the temperature 20 mm behind (i.e. were the weld gun was 2 s ago) the weld gun is shown. The data was interpolated and implicitly smoothed in order to generate a non-distorted mesh-grid. A mesh-grid line parallel to the time-temperature plane is the temperature development of a point $\sigma$ behind the weld gun. The data from the second pass (preheated baseplate, layer 4) was used. . . . .	61
7.1	Laser profilometry. The laser stripe is projected onto the intersection of the surface of the weld bead and the plane (let's define it as the xz-plane) in which the laser is. The camera is tilted by an angle $\alpha$ w.r.t. the z axis. Now, the camera sees a projection of the laser stripe into the image plane. With the fact that the laser strip can only be in the xz-plane the true xyz-coordinates can be determined. Two cameras are shown to emphasize the dependency of the resolution on the angle $\alpha$ . . . . .	70

## List of Variables

Variable	Explanation	Unit
$A_w$	Wire cross section area	$\text{mm}^2$
$A_{wb}$	Cross section area of the weld bead	$\text{mm}^2$
$A_{wb,0}$	Scaling constant for the cross section area of the weld bead	1
$b$	Model parameter. See equation (4.7)	s
$\hat{b}$	Observer gain. See equation (4.9)	1
$c[n, k] \equiv c_n$	Model parameter. See equation (4.7)	mm
$\hat{c}[n, k] \equiv \hat{c}_n \equiv \hat{c}_{n,k}$	Observer state. See equation (4.16)	mm
$e[n, k] \equiv e_n$	Observer error	mm
$e_\infty$	Limit of $e_n$ if $n \rightarrow \infty$	mm
$e_z[n, k] \equiv x[n, k]$	Layer height error w.r.t. to $z[n, k]$ and $\bar{z}[n, k]$	mm
$\eta$	Efficiency coefficient of the welding process	1
$f(y)$	Denotes that something is a function of the variable $y$	
$\Gamma_w$	Surface of a Volume through which the wire is fed (figure 3.2)	$\text{mm}^2$
$\Gamma_v$	Surface of a Volume through which the weld bead leaves the volume (figure 3.2)	$\text{mm}^2$
$H$	Heat input as energy per unit length	$\frac{\text{J}}{\text{mm}}$
$H_V$	Volumetric heat input as energy per unit volume	$\frac{\text{J}}{\text{mm}^3}$
$I_w$	Welding current	A

## List of Figures

$k$	Segment number	1
$K$	Total number of segments	1
$n$	Layer number	1
$N$	Total number of layers	1
$\Omega$	Some Volume (figure 3.2)	$\text{mm}^3$
$p$	Delay of the control action w.r.t $\Delta z$ or $A_{wb}$ as multiple of $\Delta s$	1
$p$	Relative error	%
$P_{arc}$	Arc power	W
$r$	Controller gain. See equation (4.12)	$\frac{1}{s}$
$s_k$	Position of the segment $k$ measured from the centre of the first segment of the weld bead	mm
$\Delta s$	Length of a segment. I.e. discretization step size of the position	mm
$\tau$	Delay of the control action w.r.t $\Delta z$ or $A_{wb}$	s
$U_{arc}$	Arc voltage	V
$v$	Travel Speed (TS) – velocity of the robot's tool centre point (TCP)	$\frac{\text{mm}}{s}$
$v[n, k] \equiv v_n \equiv v_{n,k}$	Travel Speed at layer $n$ and segment $k$	$\frac{\text{mm}}{s}$
$\bar{v}$	Working point for the travel speed for a linearisation	$\frac{\text{mm}}{s}$
$v_{\max}$	Upper bound on the travel speed (Controller parameter)	$\frac{\text{mm}}{s}$
$v_{\min}$	Lower bound on the travel speed (Controller parameter)	$\frac{\text{mm}}{s}$
$v_{\vartheta}$	Denotes a dependency on the temperature field	K
$\dot{V}_w$	Volume flow into $\Omega$ through $\Gamma_w$	$\frac{\text{mm}^3}{s}$
$\dot{V}_v$	Volume flow out of $\Omega$ through $\Gamma_v$	$\frac{\text{mm}^3}{s}$



$w$	Wire Feed Speed (WFS) – Wire feed in length units per unit time trough the wire feeder	$\frac{\text{mm}}{\text{s}}$
$w[n, k] \equiv w_n$	Wire Feed Speed at layer $n$ and segment $k$	$\frac{\text{mm}}{\text{s}}$
$x[n, k] \equiv x_n \equiv x_{n,k}$	Layer height error w.r.t. to $z[n, k]$ and $\bar{z}[n, k]$	mm
$\hat{x}[n, k] \equiv \hat{x}_n \equiv \hat{x}_{n,k}$	Observer state	mm
$z[n, k]$	Absolute height of the workpiece at layer $n$ and segment $k$	mm
$\bar{z}[n, k]$	Reference height of the workpiece at layer $n$ and segment $k$	mm
$\Delta z[n, k]$	Layer height at layer $n$ and segment $k$	mm
$\bar{\Delta z}[n, k]$	Reference layer height at layer $n$ and segment $k$	mm



# 1 Introduction

Due to the increasing demand on custom parts where the batch size is rather small, additive manufacturing (AM) processes experience a boost in development. Not only can near-net shaped parts be manufactured, but there is also no need for costly equipment like molds, dies and special fixtures. With additive manufacturing, parts can be manufactured in one work step and the geometry of the product can be altered without the need to physically change the setup. In aerospace, where the batch size is naturally small and the geometries are rather complex in order to reduce weight, processes which can produce net-shaped parts are especially popular. It is common for this industry to have a buy-to-fly (BTF) between 10 and 20 according to S. W. Williams et al., [2016](#). This means when you have a part which weights 1 kg you have to buy 20 kg of stock material. AM can greatly reduce this number. S. W. Williams et al., [2016](#) reports a BTF ratio of 1.2 for a wing spar made from titanium with Plasma Arc Welding.

There are four main categories of additive manufacturing with metals (Wu, Pan, et al., [2018](#)): Directed Energy Deposition, Powder Bed Fusion, Powder Jetting and Sheet Lamination. Directed Energy Deposition can be further classified by the used feedstock (wire or powder based) and energy source (laser beam, electron beam, plasma, electric arc), Dass and Moridi, [2019](#).

## 1 Introduction

---

This thesis mainly focuses on Wire Arc Additive Manufacturing (WAAM). Like the name suggests, it uses an electric arc as the heat source and a wire as filler material. Therefore, the setup is very cheap. One can use a conventional welding power source and an industrial robot or gantry to build a basic setup. Its advantages over e.g. powder bead fusion is the high deposition rate of 1 kg/h up to 8 kg/h (Wu, Pan, et al., 2018). To put it in contrast powder based processes have a deposition rate of about 0.1 kg/h up to 0.2 kg/h and a lower BTF ratio between 1.7 and 10 according to Colegrove and S. Williams, 2013. Additionally, due to the easy setup it is possible to add details on existing parts like fittings. There is also virtually no limit on the build volume. In powder bead fusion the part can only be manufactured in a confined volume that will be sequentially filled with powder and partly melted and fused to the previous layer. This means the work volume can practically not be bigger than a few meters. In WAAM, however, the robot can be mounted on a mobile solution, therefore the work volume can be extended to any size.

The process was first patented in 1926 by Baker and further developed since then (Colegrove and S. Williams, 2013). However, it is still rare to encounter a part, manufactured by WAAM despite the many advantages. This is because there are of course disadvantages. Among them are residual stresses in the workpieces, the high surface roughness due to humping and layer lines (therefore only near-net shaped), low complexity of the geometry (mainly extruded geometries). Further more, the process is not at all robust w.r.t parameter variations. This means if you use a different alloy, the parameters of the process must be adapted. Every material has to be treated special and there is no method that works for many different materials without the need for a new set of parameters. Especially different metals have different properties which lead to different challenges. Where porosity is a problem for aluminium, it is no problem at all for titanium, but with titanium there is the problem of arc wandering and

---

large columnar  $\beta$  grains S. W. Williams et al., [2016](#).

And even with the same material, after a few layers the heat dissipation changes and therefore the weld bead geometry as well as the crystal structure. It was found that thin walls produced by AM have sections of different crystalline structure due to different thermal histories of the sections, Wu, Ding, et al., [2017](#), Wu, Pan, et al., [2018](#), Dinovitzer et al., [2019](#). From this the problem of stable layer geometries arises. This thesis will focus on developing a closed loop solution to achieve stable geometries.



## 2 Literature Review

### 2.1 Welding Technologies

As mentioned in chapter 1 there are different types of additive manufacturing for metals. One of them is Directed Energy Deposition, see figure 2.1.

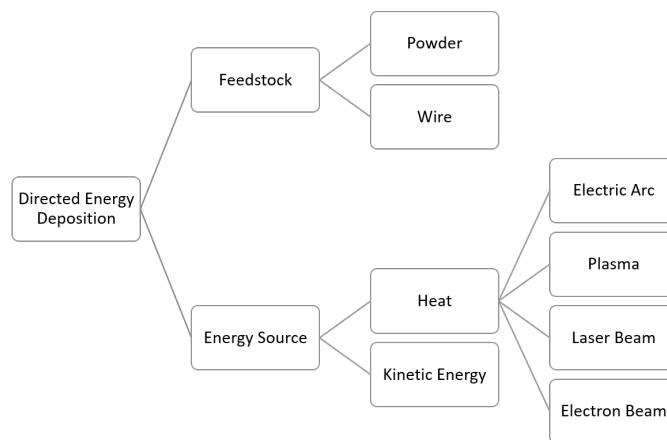


Figure 2.1: Classifications of Directed Energy Deposition processes according to Dass and Moridi, 2019

Wire Arc Additive Manufacturing (WAAM) is one of the most promis-

ing technology. It uses an electric arc as heat source and metal wire as feedstock. According to Wu, Pan, et al., [2018](#), WAAM can be further distinguished into:

- GMAW Gas Metal Arc Welding
- GTAW Gas Tungsten Arc Welding
- PAW Plasma Arc Welding

GMAW uses a consumable electrode which is the filler material. This is especially convenient, since there is no need for a separate wire feeder and therefore no additional axis to orient the wire feeder. With this technology even overhangs and horizontal beads can be welded. Although, this technology has a less stable arc and produces more spatter than e.g. GTAW according to Wu, Pan, et al., [2018](#).

A better choice is CMT which is a special case of GMAW. The wire feed as well as the current are modulated in order to move the feed stock to the workpiece "cold" and only apply heat to melt the dip. Therefore the heat input is lower, the process is nearly spatter free and the bead quality is higher according to S. W. Williams et al., [2016](#). This process is especially good for welding aluminium. Due to the lower heat input the porosity of the workpiece is greatly reduced (Derekar, [2018](#)). However, the main reason for porosity in aluminium are impurities (Wu, Pan, et al., [2018](#), S. W. Williams et al., [2016](#)). One downside of CMT and GMAW is the arc wandering. This occurs e.g. with titanium. Even though, CMT is much better than GMAW in this concern. When welding titanium with CMT the surface shows a higher roughness.

A viable option to weld titanium is PAW. A tungsten electrode produces an arc to heat up a gas which turns it into a plasma and is forced through a small orifice. The plasma acts as the heat source for the welding. The



plasma stream is highly directed and therefore no arc wandering occurs according to S. W. Williams et al., 2016. However, a separate wire feeder is needed and therefore an additional axis to orient the wire feeder.

GTAW uses a tungsten electrode as well but here the arc is directly used to create a plasma channel that heats the substrate and the filler material. Same as for PAW a external wire feeder and thus an additional axis are needed. Beside fewer arc wandering there are no major advantages of GTAW over GMAW.

## 2.2 Materials

Titanium and Aluminium are especially appealing since they are common materials for light weight applications like aerospace. With Titanium where prices as high as £100/kg to £250/kg (S. W. Williams et al., 2016) are common, a low buy-to-fly (BTF) ratio is especially advantageous. This is where WAAM is especially good at. Also machining titanium can be inconvenient due to its high strength thus tools will wear out earlier. However, titanium suffers from severe oxidation, especially in the upper layers due to heat accumulation according to Wu, Ding, et al., 2017. Also a strong anisotropy can be found - the strength in the build direction is higher. However by applying high pressure rolling the crystal structure is refined and strengths higher than that for wrought parts can be achieved, S. W. Williams et al., 2016.

Aluminium on the other hand is cheaper with £6/kg to £100/kg. Also it is easy workable and there are many processes that achieve better results than WAAM. However, for very small batch sizes or delicate alloys WAAM

can be advantageous. The main issue with aluminium is the porosity – mainly due to impurities according to Wu, Pan, et al., [2018](#).

Another group of costly and difficultly workable materials are super alloys like the nickel alloy Inconel. It is used e.g. for turbine blades. That means the weight and the BTF ratio should be minimized. With conventional methods like CNC machining BTF ratios will be an order of magnitude higher than with WAAM. Further more those nickel alloys remain extremely hard even at high temperatures, which makes it inherently hard to shape with conventional subtractive methods. However, the WAAM process has some shortcomings as well like delamination, warping and buckling, due to residual stresses in the material, Dhinakaran et al., [2020](#).

The most commonly used metal – steel – can also be used in the WAAM process. Even though, it is less advantageous than titanium or super alloys due to its low price of £2/kg to £15/kg (Derekar, [2018](#)). Also non-stainless steel has severe problems with oxidation. Steel can still be useful for prototyping, small batch sizes and geometries that can not be manufactured with conventional methods like subtractive manufacturing techniques. However, due to its low price, it is suitable for research where the material is not the main focus. This is the reason mild steel is used for the experiments in this thesis.

### 2.3 Challenges

There are two major classes of challenges in WAAM. First, process control related and second, material science related. For both, researchers primarily concentrate on single-bead multi-layer and single-bead single-layer

experiments i.e. no complex structures.

### 2.3.1 Process control challenges

With Wire Arc Additive Manufacturing (WAAM) near net-shaped parts can be manufactured. The reason to call it near net-shape is that the geometrical accuracy of WAAM processes is low (a few mm). This originates from the layer by layer build process of the parts. However, reaching desired geometries i.e. bead width and bead height is a major concern of research. Many methods are proposed to achieve a desired geometry.

Among them closed-loop control of the travel speed to achieve a desired bead width (Xiong, Yin, and W. Zhang, 2016) or control of the wire feed speed and travel speed to achieve a desired bead width and height (Doumanidis and Kwak, 2002) or control of the nozzle to top surface distance (NTSD). All approaches model the system as a continuous system with one or both of the inputs travel speed, wire feed speed and the geometry as output quantity. Problems arise at the start and the end of the weld.

Another approach to achieve a given geometry is to create an accurate lookup table of the deposition as a function of the process parameters. By doing so labour expensive experiments must be conducted for each setup and material and also for different geometries.

Beside the overall geometry the surface finish is important. If the travel speed is too high, humping occurs Adebayo, 2013. Humping are waves in the layer along the weld direction.

With such a difficult process, the tool path planning is an important research area as well. By choosing the tool path always in the same direction stresses occur and can lead to severe deformations. To counteract this tool path directions can be alternated or parts can be generated back to back in order to apply the same stresses on both sides to cancel each other Derekar, 2018. In general the path planning must predict and counteract the deformation during the process.

At the start and at the end of each bead the process can not be conducted as usual and also the models don't apply therefore start and stop strategies have to be developed to achieve the desired geometry in those regions. In general there is a bulge at the start due to the good cooling from the cold underlying layer and a scallop at the end where no more material is added and the weld bead solidifies in place.

For thin wall experiments there are 3 zones with different material properties: the lower zone which went through the strongest temperature gradient due to the base plate, the middle zone which is the main part and the upper zone which went through a strong temperature gradient as well due to air and the missing reheating cycles. In Li et al., 2018 was shown that thermoelectric cooling can help to achieve more uniform thermal cycles for each layer which results in more uniform bead geometries as well.

### 2.3.2 Material related challenges

Depending on which material is used different defects arise. For example aluminium is prone to porosity which is primarily caused by impurities or surface contaminations in the stock material. Although, this can be

reduced by a lower heat input like in CMT-PADV and using high quality feedstock as well as clean environments Wu, Pan, et al., 2018. Also the presence of alloying elements can cause porosity Derekar, 2018.

Adebayo, 2013 states the following reasons for porosity:

- Insufficient flow rate of shielding gas
- Surface oxidation or other contamination
- Inappropriate parameters
- Too high travel speeds
- Presence of impurities such as phosphorus or sulphur on feedstock

A major challenge is the treatment or avoidance of residual stresses. Those are associated with the shrinkage during cooling and are large along the weld direction S. W. Williams et al., 2016. The residual stress is the stress that remains in the material when all external loading forces are removed. If the stress in the material is higher than the ultimate tensile strength cracking will appear. And if it is between the yield strength and the ultimate tensile strength warping or plastic deformation occurs. So, residual stress leads to various other problems like delamination, warping, cracking as well as it reduces the fatigue performance and the fracture resistance Wu, Pan, et al., 2018. Path planning must be conducted accordingly. Especially bimetal parts are prone for residual stresses due to the inherently big difference in thermal expansion between the materials. To counteract, accurate control of the interpass temperature is needed. Another approach is the back to back technique where the WAAM part is created on both sides of the substrate or symmetrical building where material is added in a way to balance out the introduced stresses around a symmetry plane. Also the part orientation can have an influence on the stresses, in general shorter paths produce less stresses.

As mentioned above residual stress leads to deformation which reduces

accuracy of the process as well as the buy-to-fly ratio because more material has to be removed to obtain the desired part. I.e. a slightly curved wall must be thick enough such that there is still a straight core with the desired dimensions. There are several forms of deformation like bending, twisting, shrinkage and angular distortions.

Cracking and delamination occur if the stress is higher than the ultimate tensile strength of the material. Parts that have cracks or delaminations cannot be used any more. Therefore, those defects have to be monitored accurately e.g. after the process with non-destructive tests.

### 2.4 Ancillary Processes

In order to reduce defects, improve material properties or homogeneity ancillary processes are used. Those are modifications of the basic WAAM process to alter e.g. the temperature gradient in the metal, the thermal history or introduce vibration, in general oscillations in some quantities to refine the microstructure, geometry or stability of the process and so on.

One very promising technique is interpass rolling. After each layer a high pressure is applied, thus introducing stress into the material which – after reheating – refines the grain size towards smaller randomly oriented homogeneously sized grains. Therefore, the material becomes more isotropic and harder. Also residual stresses and porosity can be reduced (Wu, Pan, et al., 2018). One shortcoming of this technique are the high forces and the constraint on geometries. Rolling can only be applied on easy geometries, like walls or flat surfaces with no overhangs or pockets underneath. Otherwise the workpiece could be deformed or the roller could be unable

to reach all surfaces.

The same effect on the grains can be achieved with peening and ultrasonic impact treatment. Those techniques impose high stresses on the weld surface in order to refine the grain structure. However, the effect is only on the surface (to a depth of 1 mm-2 mm for peening and around 60  $\mu\text{m}$  for ultrasonic impact treatment according to Wu, Pan, et al., 2018).

Since the main reason for columnar grain growth is the temperature gradient, many ancillary processes aim to control the temperature distribution through e.g. active cooling. Li et al., 2018 found that cooling of thin walls can produce smaller grains and also improve the homogeneity of the wall. Also the geometrical accuracy can be improved since the temperature gradient is kept constant throughout the build process, thus eliminating heat accumulation and therefore the varying shape of the weld bead.

Also heating of the workpiece in front or behind the weld pool can create a more uniform temperature distribution both in space and in time according to Cunningham et al., 2018. Thus reducing the temperature gradient and therefore the residual stresses. Wire heating can reduce the needed energy to melt the wire which leads to a reduced width of the weld bead, better cooling and a better weld pool mixing (Cunningham et al., 2018).

Heat accumulation causes a loss of geometrical accuracy and therefore interpass cooling was introduced. By letting the workpiece cool down to a specified temperature between passes the geometrical accuracy of the weld bead can be greatly improved. The first layers experience a strong temperature gradient, since the base plate can be assumed to have a constant temperature and therefore acts as a good heat sink. This leads to thinner and higher weld beads. But after a few layers the heat dissipation

through the small cross section of the wall leads to a smaller temperature gradient. This means the temperature of the top layer is elevated and consequently the weld bead gets smaller in height and wider. Now, if the next pass starts immediately after the previous, the heat in the upper section is not yet dissipated and it will accumulate over the process, which means the temperature will rise with higher layer numbers as shown by Wu, Ding, et al., 2017. By introduction the interpass dwell time i.e. interpass cooling, the temperature of the top layer is always the same before starting the next pass. Therefore, the temperature gradient for each subsequent layer is similar and therefore the weld bead geometry as well. This method can be implemented by only adding a pyrometer and the effect is significant. Now, one question is, if the temperature of the weld pool stays the same throughout one pass or if it changes due to a changing temperature field which further leads to change in the geometry of the weld bead. This question is treated in chapter 5.7.

Another class of ancillary processes are oscillation based ones. According to Cunningham et al., 2018, modulating the current can decouple the material transfer from the base plate heating process, thus reducing the overall heat input. Further the oscillations in the current can excite the resonance frequency of the weld pool which introduces additional stirring thus improving the grain formation. However, operating at exactly the resonance frequency of the weld pool (10 Hz to 200 Hz) can lead to the loss of geometrical accuracy.

Fronius has developed a nearly spatter free process called Cold Metal Transfer (CMT). The wire is transferred to the weld pool cold, thus creating a short-circuit which usually creates spatters. But in CMT the short-circuit is detected and the current is reduced to avoid spatters. To improve the droplet detachment at this reduced current, the wire feeder retracts the wire in the moment of the short-circuit. The process reduces the heat input



and the spattering.

Direct weld pool oscillation introduced by Lorenz Forces with an oscillating magnetic field yielded improved grain refinement and thus higher strengths. There are many other experiments that showed that a stirring of the weld pool improves the grain refinement (Cunningham et al., [2018](#)).

Finally, if the geometrical accuracy of the weld bead is too low, CNC machining can be applied i.e. additive subtractive manufacturing. With this technique, small features that are no longer accessible after completing the build can be added and surface finished during the build process, like e.g. cooling channels.



## 3 Problem

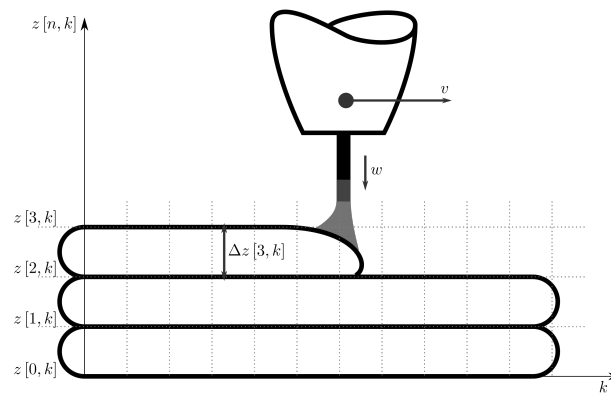


Figure 3.1: Gas Metal Arc Welding (GMAW) and its quantities.  $w$  ... Wire feed speed.  
 $v$  ... Travel speed.  $z[n, k]$  ... height of layer number  $n$  at position number  $k$ .

### 3.1 Significant quantities

Let's start with an overview of the quantities that influence the process the most. According to Singh, Sharma, and Rathod, [2021](#) the process parameters with the most influence on the process are

- Welding current (A)

### 3 Problem

---

- Arc voltage (V)
- Travel speed ( $\frac{m}{s}$  but usually  $\frac{mm}{s}$  or  $\frac{m}{min}$ )
- Wire feed speed ( $\frac{m}{s}$  but usually  $\frac{mm}{s}$  or  $\frac{m}{min}$ )
- Wire electrode extension (m but usually mm)
- Interpass temperature.

The welding current is the most important parameter for the bead geometry. It controls the electrode burn off which directly couples this quantity to the wire feed speed (WFS) (i.e. the WFS cannot be chosen without altering the welding current). Furthermore, the welding current determines the fusion depth and therefore is closely connected to material properties. The heat input is direct proportional to the weld current and therefore the weld pool dimensions and the bead geometry.

The wire feed speed (WFS) is the length of the added stock material (wire) per unit time. It is closely connected to the cross-section area and the heat input.

The travel speed (TS) is the velocity of the tip of the weld gun with reference to the workpiece. If the travel speed is too high humping occurs (visible waviness in the surface along the welding direction). Furthermore, the travel speed affects the penetration depth and the bead size. Also if the travel speed is too high the material may experience the shield gas for a too short period and oxidation occurs.

Adebayo, 2013 pointed out that keeping the ratio  $\frac{WFS}{TS}$  constant results in a constant cross section even if TS and WFS changes (as long as the ratio stays the same). Wire feed speed will be denoted by  $w$  and the travel speed as  $v$ . Let's consider a box  $\Omega$  around the weld pool that is fixed relative to the weld gun. The only areas where material is introduced are the surfaces  $\Gamma_w$  and  $\Gamma_v$  (see figure 3.2). The volume flow  $\dot{V}_w$  into the surface  $\Gamma_w$  can be

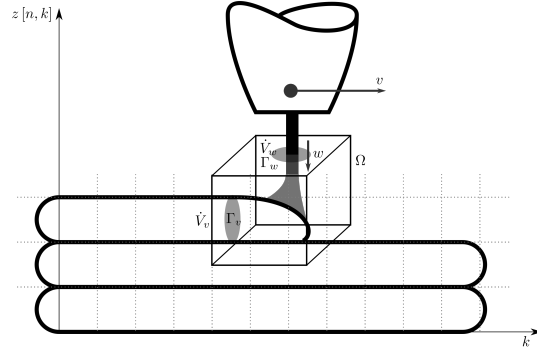


Figure 3.2: The volume flow  $\dot{V}_w$  into the volume  $\Omega$  must be same as the volume flow  $\dot{V}_v$  out of it – otherwise material would accumulate.

calculated with the WFS  $w$  and the cross section area of the wire which will be denoted by  $A_w$ .

$$\dot{V}_w = w \cdot A_w \quad (3.1)$$

And the volume flow  $\dot{V}_v$  out of the surface  $\Gamma_v$  can be calculated in a similar manner with the travel speed  $v$  and the cross section area of the weld bead denoted by  $A_{wb}$ .

$$\dot{V}_v = v \cdot A_{wb} \quad (3.2)$$

Now, this two volume flows must be equal  $\dot{V}_v \stackrel{!}{=} \dot{V}_w$ , otherwise material would accumulate inside the volume  $\Omega$ . We assume a steady state and therefore no accumulation inside the volume  $\Omega$ . This yields

$$A_{wb} = A_w \cdot \frac{w}{v}. \quad (3.3)$$

Let's further assume that the cross section area has an arbitrary shape which can be represented by a single bounding curve  $f(y)$ . The cross

### 3 Problem

---

section area is

$$A_{wb} = \int_{y_0}^{y_1} f(y) dy.$$

If we want to scale the area in both dimensions we can write this as

$$A_{wb}(p) = \int_{y_0 \cdot p}^{y_1 \cdot p} f\left(\frac{y}{p}\right) \cdot p dy$$

which is equivalent to

$$A_{wb}(p) = \int_{y_0 \cdot p}^{y_1 \cdot p} f\left(\frac{y}{p}\right) \cdot p dy \stackrel{v = \frac{y}{p}, dy = p \cdot dv}{=} p^2 \cdot \int_{y_0}^{y_1} f(v) dv.$$

So, the area always scales with the square of the scaling factor  $p$ . Now, let's consider  $\max_y \{f(y)\} \stackrel{!}{=} 1$  therefore the scaling factor becomes the layer height  $\Delta z$ . In other words

$$A_{wb} = A_{wb,0} \cdot \Delta z^2. \quad (3.4)$$

Thus the layer height  $\Delta z$  can be written in terms of travel speed  $v$  and wire feed speed  $w$  as

$$\Delta z = \sqrt{\frac{A_w}{A_{wb,0}}} \cdot \sqrt{\frac{w}{v}}. \quad (3.5)$$

As long as the cross section shape stays the same we have a very good model for the layer height. This model is validated in chapter 5.

The wire electrode extension is the length of the wire between the contact tip and the end of the wire where the arc is generated. If this quantity is too large the bead will be poorly shaped and the process has a low penetration. Also shielding will be harder and oxygen could reach the workpiece earlier for larger values.

The arc voltage is the potential difference between the tip of the electrode and the top surface of the workpiece. Together with the weld current the transient power input can be calculated. With both the welding current and the travel speed the heat input can be estimated.

In literature the arc power is commonly calculated as the product of welding current  $I_w$  and the arc voltage  $U_{arc}$  (let's assume RMS values)

$$P_{arc} = U_{arc} I_w.$$

The heat input according to Joseph, 2001 is

$$H = \eta \cdot \frac{P_{arc}}{v}$$

where  $\eta$  is the efficiency of the process and  $v$  is the travel speed.  $H$  is a quantity of (heat) energy per unit length i.e. the energy input for each unit length of the weld bead.

Let's introduce a new quantity, the volumetric heat input which is the introduced energy per unit volume

$$H_V = \eta \cdot \frac{P_{arc}}{v A_{wb}}$$

Or with equation (3.3)

$$\boxed{H_V = \frac{\eta}{A_w} \cdot \frac{I_w \cdot U_{arc}}{w}}. \quad (3.6)$$

So, by reducing the wire feed speed the volumetric heat input increases, which leads to a higher temperature, which consequently means a higher weld pool temperature. Thus, this would lead to a weld bead that is smaller in height and wider. But only if the current  $I_w$  stays the same!

### 3 Problem

---

Also, this model is yet to be validated but this will not be done in this thesis. However, the CMT process dynamically adjusts the current in order to match the wire feed speed i.e. synergic power supply, therefore it will not be easily possible to validate this model using CMT.

The workpiece temperature cannot be easily monitored continuously. For this reason the workpiece temperature distribution is dropped in favor of the interpass temperature. The interpass temperature is the average temperature of the topmost layer just before the next pass.

Ambient conditions such as temperature and humidity should not have an effect due to the presence of shielding gas.

Beside the process parameters the following quantities are of major interest:

- Bead height
- Bead width
- Material properties

Achieving a given bead geometry i.e. bead height and bead width is the basis of a WAAM process. After reaching this goals the process can be steered towards certain material properties.

If all of the significant welding parameters as well as the output quantities are monitored, the experiments gain a better repeatability and effects occurring during the process can be described better.



## 3.2 Accessible quantities

In this thesis a specific setup will be used. Only one quantity is monitored and only one can be controlled. The setup consists of a CMT welding power source from Fronius as well as the torch and an ABB robot. All the programming is done on the ABB robot. Therefore, not all quantities from the welding process are accessible. The setup will be explained in more detail in chapter 5.

The only quantity that is measured is the layer height. This is done by moving the torch over a point and lowering it until it touches the workpiece and closes the electric circuit. Unfortunately, at the time it was not possible to monitor any temperature. It was also not possible to monitor the arc voltage, the welding current nor the wire feed speed. The wire feed speed was set once and never changed again.

The only quantity that we will regulate is the travel speed.

## 3.3 Problem statement

This thesis focuses on a control strategy to regulate the absolute height of each layer by adjusting the travel speed. The only measurement quantity is the absolute height of each layer measured after the welding process of each pass. More specific, the goal is to achieve a levelled top layer surface i.e. no curvature and no humping.

As mentioned earlier it is essential to achieve a stable bead geometry in or-

der to manufacture parts with GMAW (or more specific CMT in this case). In current research many papers are dedicated to this topic. However, researchers regulate the bead geometry below the weld gun by adjusting the wire feed speed or travel speed. The controller is designed in continuous time and also an continuous measurement of the layer geometry is necessary. Start and stop strategies can not easily be implemented.

Xiong and G. Zhang, [2014](#) regulate the nozzle to top surface distance by adjusting the wire feed speed by using an adaptive linear continuous time model for the process. In another paper Xiong, Yin, and W. Zhang, [2016](#) model the system with a Hammerstein system i.e. a polynomial approximation of the dynamics of the system, and control the layer width. Doumanidis and Kwak, [2002](#) proposed a strategy to control both the layer width and height as well as the temperature field in order to achieve certain material properties.

Yet, all approaches require a continuous measurement of the geometry. This is either done with complex camera systems or laser gauging. In this thesis, no such measurement is available and the geometry (i.e. here the layer height) can only be obtained after a pass.

## 4 Solution

### 4.1 Model

First, let's recap our knowledge so far. From equation (3.5) and equation (3.6) we have

$$\Delta z = \sqrt{\frac{A_w}{A_{wb,0}}} \cdot \sqrt{\frac{w}{v}}$$
$$H_V = \frac{\eta}{A_w} \cdot \frac{I_w \cdot U_{arc}}{w}.$$

Equation (3.5) assumes a non-changing cross section shape. But the shape strongly depends on the temperature field. It is expected that with higher layers the temperature gradient will be smaller and the weld pool temperature higher, thus a wider weld bead and therefore a changing cross section shape. With this in mind let's rewrite equation (3.5) as

$$\Delta z = f\left(\sqrt{\frac{w}{v}}, \nu_\vartheta\right) \quad (4.1)$$

where  $\nu_\vartheta$  is a disturbance that depends on the temperature field. This quantity remains unknown since the temperature is not measured. It can be assumed that it is slowly varying.

From equation (3.6) we could make assumptions about the temperature but the welding current and the arc voltage are not measured, therefore this relation is dropped.

The layer height is only measured after a pass, therefore the following representation of the system is proposed. We assume a thin single bead wall with  $N$  subsequent layers. The bead will be discretised into  $K$  segments of equal length  $\Delta s$ . Therefore the layer height becomes  $\Delta z = \Delta z[n, k]$  where  $n$  is the currently build layer and  $k$  is the segment number ( $n = 0, 1, \dots, N - 1$  and  $k = 0, 1, \dots, K - 1$ ).

Xiong and G. Zhang, 2014 as well as Dumanidis and Kwak, 2002 considered a delay in  $\Delta z$  w.r.t.  $w$  or  $v$  since the control action is delayed by a Low-Pass behaviour. Therefore, we will use equation (3.3) to derivate a model for the delay. In figure 4.1 a qualitative explanation is given.

$$A_{wb}(s) = A_w \cdot \frac{w(s - \tau)}{v(s - \tau)}$$

Due to the discretization of the model we will need the average of the cross section area over a segment, therefore

$$\bar{A}_{wb}[n + 1, k] = \frac{1}{\Delta s} \cdot \int_{k \cdot \Delta s}^{(k+1) \cdot \Delta s} A_w \cdot \frac{w(s - \tau)}{v(s - \tau)} ds.$$

We assume  $v[n, k]$  and  $w[n, k]$  are constant over a segment. Further we assume a constant delay of  $\tau = p \cdot \Delta s$  with  $0 \leq p < 1$ . So, we can split the integral into

$$\begin{aligned} \bar{A}_{wb}[n + 1, k] &= \frac{A_w}{\Delta s} \cdot \int_{k \cdot \Delta s}^{(k+p) \cdot \Delta s} \frac{w(s - \tau)}{v(s - \tau)} ds + \int_{(k+p) \cdot \Delta s}^{(k+1) \cdot \Delta s} \frac{w(s - \tau)}{v(s - \tau)} ds \\ &= \frac{A_w}{\Delta s} \cdot \int_{k \cdot \Delta s}^{(k+p) \cdot \Delta s} \frac{w[n, k - 1]}{v[n, k - 1]} ds + \int_{(k+p) \cdot \Delta s}^{(k+1) \cdot \Delta s} \frac{w[n, k]}{v[n, k]} ds \\ &= A_w \cdot \left( p \frac{w[n, k - 1]}{v[n, k - 1]} + (1 - p) \frac{w[n, k]}{v[n, k]} \right). \end{aligned}$$

And in terms of  $\Delta z$  the model can be written as

$$\Delta z[n+1, k] = \sqrt{\frac{A_w}{A_{wb,0}}} \cdot \sqrt{p \frac{w[n, k-1]}{v[n, k-1]} + (1-p) \frac{w[n, k]}{v[n, k]}}. \quad (4.2)$$

With the assumptions in equation (4.1) the model can be written as

$$\Delta z[n+1, k] = f \left( \sqrt{p \frac{w[n, k-1]}{v[n, k-1]} + (1-p) \frac{w[n, k]}{v[n, k]}}, \nu_\theta \right). \quad (4.3)$$

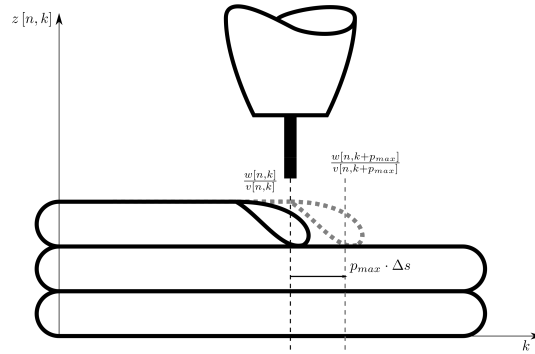


Figure 4.1: The control action will be delayed due to the finite dimensions of the weld pool. Only after one full length of the weld pool, it can be assumed that the control action took full effect. However, we can estimate the delay in the model by half the length of the maximal delay  $p_{max}$  which means the control action is halfway executed.

Until now, we always focused on the layer height but the goal is to achieve flat layer surfaces. Therefore, we have to consider the deviations from the reference height of the previous layer as well. Let's denote the absolute height of the layer  $n$  at position  $k$  with  $z[n, k]$  and the reference with  $\bar{z}[n, k]$ . The difference of the reference heights should be constant with  $\bar{z}[n, k] = \bar{\Delta z} \cdot n$ . Additionally, let's define the error from the reference as

## 4 Solution

---

$$e_z[n, k] = z[n, k] - \bar{z}[n, k].$$

$$z[n+1, k] = z[n, k] + \Delta z[n+1, k] \stackrel{!}{=} \bar{z}[n+1, k] = \underbrace{\bar{z}[n, k]}_{z[n, k] - e_z[n, k]} + \overline{\Delta z}$$

Which yields

$$\Delta z[n+1, k] \stackrel{!}{=} \overline{\Delta z} - e_z[n, k] \quad (4.4)$$

as the control goal.

The system can also be written in terms of  $e_z$ .

$$\begin{aligned} e_z[n, k] &= z[n, k] - \bar{z}[n, k] \\ e_z[n+1, k] &= z[n+1, k] - \bar{z}[n+1, k] = \Delta z[n+1, k] + z[n, k] - \overline{\Delta z} - \bar{z}[n, k] \end{aligned}$$

which is

$$e_z[n+1, k] = e_z[n, k] + \Delta z[n+1, k] - \overline{\Delta z}$$

(4.5)

and the control goal becomes

$$e_z[n+1, k] \stackrel{!}{=} 0$$

.

## 4.2 Controller design

Since, we don't know  $f(\cdot)$  in equation (4.3), a Taylor Series expansion will be done and the factors will be assumed to be constant unknowns. Terms

of order two or higher will be neglected.

$$\begin{aligned}
 f\left(\sqrt{p \frac{w[n, k-1]}{v[n, k-1]} + (1-p) \frac{w[n, k]}{v[n, k]}}, v_\theta\right) &= f\left(\sqrt{\frac{\bar{w}}{\bar{v}}}, \bar{v}_\theta\right) \\
 &+ \left.\frac{\partial f}{\partial v[n, k-1]}\right|_{\bar{v}, \bar{v}_\theta} (v[n, k-1] - \bar{v}) + \left.\frac{\partial f}{\partial v[n, k]}\right|_{\bar{v}, \bar{v}_\theta} (v[n, k] - \bar{v}) \\
 &+ \left.\frac{\partial f}{\partial v_\theta}\right|_{\bar{v}, \bar{v}_\theta} \Delta v_\theta
 \end{aligned}$$

The wire feed speed  $w$  will be assumed constant  $\bar{w}$ .  $\bar{v}$  is the point around which the function should be approximated.  $\Delta v_\theta$  is the deviation from a average  $v_\theta = \bar{v}_\theta$  at  $\bar{v}$ .

By replacing the derivatives at  $\bar{v}$  with constants the model w.r.t  $e_z$  is

$$e_z[n+1, k] = e_z[n, k] + a_0 v[n, k] + a_1 v[n, k-1] + a_2 \quad (4.6)$$

with

$$\begin{aligned}
 a_0 &= \left.\frac{\partial f}{\partial v[n, k]}\right|_{\bar{v}, \bar{v}_\theta} \\
 a_1 &= \left.\frac{\partial f}{\partial v[n, k-1]}\right|_{\bar{v}, \bar{v}_\theta} \\
 a_2 &= -\bar{\Delta z} + f\left(\sqrt{\frac{\bar{w}}{\bar{v}}}, \bar{v}_\theta\right) - \left(\left.\frac{\partial f}{\partial v[n, k]}\right|_{\bar{v}, \bar{v}_\theta} + \left.\frac{\partial f}{\partial v[n, k-1]}\right|_{\bar{v}, \bar{v}_\theta}\right) \bar{v} + \left.\frac{\partial f}{\partial v_\theta}\right|_{\bar{v}, \bar{v}_\theta} \Delta v_\theta.
 \end{aligned}$$

This means  $a_2$  is slowly varying with time since  $v_\theta$  is slowly varying with time. If  $e_z[n, k]$  is positive it means the absolute height is bigger than the reference.

Even though, the delay  $p$  has an inevitable influence on the dynamic of the system, it was unfortunately not considered in the experiments. For this reason we will use a simplified model for the controller derivation.

$$x[n+1, k] = x[n, k] + b \cdot v[n, k] + c[n, k] \quad (4.7)$$

where  $x[n, k] = e_z[n, k] = z[n, k] - \bar{z}[n, k]$ ,  $b = a_0$ ,  $a_1 = 0$  and  $c[n, k] = c = a_2$ . The dependence of  $n$  and  $k$  in  $c$  remains in this model, since it will be assumed that  $c$  varies over  $n$  and  $k$ . Experiments showed that there is a hump at the start and a scallop at the end of a weld bead, therefore  $c$  will be assumed slowly varying over  $n$  and independent w.r.t  $k$ . Which means  $c[n, k]$  is independent of  $c[n, k+1]$  and  $c[n, k] \approx c[n+1, k]$ .

### 4.3 Observer error based controller

The position  $k$  is independent of any other position  $j$  with  $k \neq j$ , therefore the dependency  $k$  can be dropped and the dependency on  $n$  will be written in the subscript. System:

$$x_{n+1} = x_n + b \cdot v_n + c \quad (4.8)$$

Observer:

$$\hat{x}_{n+1} = \hat{x}_n + b \cdot v_n + \hat{b} \cdot (x_n - \hat{x}_n) \quad (4.9)$$

$x_n$  can be measured. Now, we can calculate the observer error

$$e_n := x_n - \hat{x}_n \quad (4.10)$$

$$e_{n+1} = e_n + c - \hat{b} \cdot e_n. \quad (4.11)$$



Calculating the steady state error yields

$$\begin{aligned}\lim_{n \rightarrow \infty} \{e_{n+1}\} &= \lim_{n \rightarrow \infty} \{e_n + c - \hat{b} \cdot e_n\} \\ e_\infty &= e_\infty + c - \hat{b} \cdot e_\infty \\ e_\infty &= \frac{1}{\hat{b}} \cdot c.\end{aligned}$$

Let's choose

$$v_n = -r \cdot (e_\infty + \hat{x}_n) - \frac{\hat{b}}{b} \cdot e_\infty \quad (4.12)$$

and calculate the steady state value of  $x_n$

$$\begin{aligned}\lim_{n \rightarrow \infty} \{x_{n+1}\} &= x_\infty = \lim_{n \rightarrow \infty} \{x_n + b \cdot v_n + c\} \\ &= \lim_{n \rightarrow \infty} \left\{ x_n - b r (e_\infty + \hat{x}_n) - \hat{b} e_\infty + c \right\} \\ &= x_\infty - b r \underbrace{(e_\infty + \hat{x}_\infty)}_{\substack{=x_\infty \\ \vdots}} - \underbrace{\hat{b} e_\infty + c}_{\substack{=0 \\ \vdots}}\end{aligned}$$

which leads to  $x_\infty = (1 - b r) \cdot x_\infty$  for which the only solution

$$x_\infty = 0$$

is. This only holds if the system is asymptotically stable because the limit wouldn't exist otherwise.

$e_\infty$  is unknown and is simply estimated by  $x_n - \hat{x}_n$ .

$$v_n = -r \cdot x_n - \frac{\hat{b}}{b} \cdot (x_n - \hat{x}_n). \quad (4.13)$$

Therefore,  $\hat{x}_{n+1}$  evaluates to

$$\hat{x}_{n+1} = \hat{x}_n - b \cdot r \cdot x_n. \quad (4.14)$$

Summary:

$$\begin{aligned}v_n &= -r \cdot x_n - \frac{\hat{b}}{b} \cdot (x_n - \hat{x}_n) \\ \hat{x}_{n+1} &= \hat{x}_n - b \cdot r \cdot x_n\end{aligned}$$

Note:  $b$  is most certainly negative!

### 4.3.1 Stability

We have the model

$$\begin{aligned}x_{n+1} &= x_n + b v_n + c \\ \hat{x}_{n+1} &= \hat{x}_n + b v_n + \hat{b} (x_n - \hat{x}_n) \\ v_n &= -r x_n - \frac{\hat{b}}{b} (x_n - \hat{x}_n)\end{aligned}$$

Let's replace  $\hat{x}_n$  with the error  $e_n = x_n - \hat{x}_n$ , this yields

$$\begin{bmatrix} x_{n+1} \\ e_{n+1} \end{bmatrix} = \underbrace{\begin{bmatrix} 1 - b r & -\hat{b} \\ 0 & 1 - \hat{b} \end{bmatrix}}_A \begin{bmatrix} x_n \\ e_n \end{bmatrix} + \begin{bmatrix} 1 \\ 1 \end{bmatrix} c$$

The values on the main diagonal of  $A$  are the eigenvalues. For a system to be asymptotically stable the dynamic matrix  $A$  must be a Schur Matrix. That means all eigenvalues are inside the unit circle. For this system it means

$$\begin{aligned}0 &< b r < 2 \\ 0 &< \hat{b} < 2.\end{aligned}$$

Note that this procedure generally works for any linear system, that means the controller design and the observer design can be done separately.

### 4.3.2 Discussion

The controller design is similar to the one done in the lecture “Prozessautomatisierung” by Horn, 2019 to remove a constant disturbance.

What does the observer state  $\hat{x}_n$  represent? From  $e_n = x_n - \hat{x}_n$  we get  $\hat{x}_n = x_n - e_n$ . And if we assume steady state which is  $x_n = x_\infty = 0$  then we get  $\hat{x}_\infty = -e_\infty = -\frac{1}{\hat{b}} \cdot c$ . So, in steady state the observer gives a measure for the constant disturbance.

Is it appropriate to assume  $e_\infty = x_n - \hat{x}_n$ ? Since, the controller is asymptotically stable this term will only bother in the transient phase and will converge to the ideal value asymptotically.

Is there a bad choice for  $br$  and  $\hat{b}$ ? Yes, if  $br > 1$  then  $x_n$  will change sign in every step, this will lead to an undesirable uneven surface on the weld bead. Or if  $br = 1$  and  $e_n = \frac{1}{\hat{b}} c$  then the controller would drive the state  $x_n$  in one step to zero – which is a very aggressive control strategy and should be avoided since the model is not ideal and also the control value  $v_n$  is tightly constraint. A better choice for example would be  $br = \frac{2}{3}$  and  $\hat{b} = \frac{4}{5}$ .

### 4.3.3 Implementation

We have the system  $x[n+1, k] = x[n, k] + b \cdot v[n, k] + c[n, k]$ . The controller is designed for one segment. In order to implement this controller we have to implement the controller for every position. The only parameters that the controllers share is  $b$ ,  $\hat{b}$  and  $r$  but not  $c$ .

How do we obtain the parameter  $b$ ? From equation (4.6) and (4.7) we know that

$$x[n+1, k] = x[n, k] + b v[n, k] + c$$

$$b = \left. \frac{\partial f}{\partial v[n, k]} \right|_{\bar{v}, \bar{v}_\theta}.$$

Further, if we assume a constant temperature in the weld pool we can use equation (4.2)

$$f(.) = \sqrt{\frac{A_w}{A_{wb,0}}} \cdot \sqrt{p \frac{w[n, k-1]}{v[n, k-1]} + (1-p) \frac{w[n, k]}{v[n, k]}}$$

and with  $p = 0$  we get

$$f(.) = \sqrt{\frac{A_w}{A_{wb,0}}} \cdot \sqrt{\frac{w[n, k]}{v[n, k]}}$$

which gives us

$$\left. \frac{\partial f}{\partial v[n, k]} \right|_{\bar{v}} = -\sqrt{\frac{A_w}{4 A_{wb,0}}} \cdot \sqrt{\frac{w}{\bar{v}^3}}.$$

This expression can be written in terms of  $f(v)$  and yields

$$b = \left. \frac{\partial f}{\partial v[n, k]} \right|_{\bar{v}} = -\frac{f(\bar{v})}{2 \bar{v}}. \quad (4.15)$$

Which means the minimum requirement to obtain the parameter  $b$  is one measurement of the height of the weld bead, welded with a travel speed of  $\bar{v}$ .

A more robust approach would be to experiment with the travel speed i.e. weld several beads with different travel speeds and approximate the dependency of  $\Delta z$  on  $v$  with a linear function. The derivative w.r.t.  $v$  is the parameter  $b$ .

## 4.4 Disturbance Observer Based Controller

The following system will be considered

$$\begin{aligned} x_{n+1} &= x_n + b \cdot v_n + c_n \\ c_{n+1} &= c_n. \end{aligned} \quad (4.16)$$

We want to design an reduced observer for the state  $c_n$ .

$$\hat{c}_{n+1} = \hat{c}_n + \hat{b} (x_{n+1} - x_n - \hat{c}_n - b v_n) \quad (4.17)$$

Note  $c_n = x_{n+1} - x_n - b v_n$ , therefore the innovation term in (4.17) is  $c_n - \hat{c}_n$ .

This can be seen as the final result of the derivation and is implemented on the robot like this. The advantage of this form is that for the estimation of  $\hat{c}_{n+1}$  any difference between the calculated  $c_n$  and  $\hat{c}_n$  can be used.

Which means if the weld direction is alternating, the following control law can be used

$$\hat{c}_{n+1,k} = \hat{c}_{n,k} + \hat{b} ((x_{n+1,K-k+1} - x_{n,K-k+1} - b v_{n,K-k+1}) - \hat{c}_{n,k})$$

With  $k = 1, 2, \dots, K$  where  $K$  is the number of sections of the trajectory.

### 4.4.1 Further derivation

In (4.17)  $x_{n+1}$  is needed. To overcome this problem a new variable is introduced  $y_n = \hat{c}_n - \hat{b} x_n$ .

$$\begin{aligned} y_{n+1} &= (1 - \hat{b}) y_n - \hat{b}^2 x_n - b \hat{b} v_n \\ \hat{c}_n &= y_n + \hat{b} x_n \end{aligned} \quad (4.18)$$

### 4.4.2 State controller

The target is to make  $x_n = 0$  asymptotically stable.

This is done by  $v_n = -\frac{1}{b} \hat{c}_n - r x_n$ .

The overall system evaluates to

$$x_{n+1} = (1 - b r) x_n + c - \hat{c}_n. \quad (4.19)$$

### 4.4.3 Stability

To proof stability, we make use of the fact that the controller and the observer can be designed separately. Starting with the observer we have

$$\begin{aligned} c_{n+1} &= c_n \\ \hat{c}_{n+1} &= \hat{c}_n + \hat{b} (c_n - \hat{c}_n). \end{aligned}$$

The observer error  $e_n = c_n - \hat{c}_n$  has the following dynamic

$$e_{n+1} = e_n - \hat{b} e_n = (1 - \hat{b}) e_n.$$

The error will asymptotically converge to zero if and only if

$$0 < \hat{b} < 2.$$

For the controller we get

$$\begin{aligned} x_{n+1} &= x_n + b v_n + c \\ v_n &= -\frac{1}{b} c - r x_n \end{aligned}$$

which yields

$$x_{n+1} = (1 - br) x_n.$$

From this we conclude that the system is asymptotically stable if and only if

$$0 < br < 2.$$

### 4.4.4 Summary

$$\begin{aligned} \hat{c}_{n+1} &= \hat{c}_n + \hat{b} (x_{n+1} - x_n - \hat{c}_n - b v_n) \\ v_n &= -\frac{1}{b} \hat{c}_n - r x_n \end{aligned} \quad (4.20)$$

with  $0 < \hat{b} < 2$  and  $0 < br < 2$ .

For the use at the robot with alternating weld directions:

$$\begin{aligned} \hat{c}_{[n+1,k]} &= \begin{cases} \hat{c}_{[n,k]} + \hat{b} \left( (x_{[n+1,K-k+1]} - x_{[n,K-k+1]} - b v_{[n,K-k+1]}) - \hat{c}_{[n,k]} \right) & n \text{ even} \\ \hat{c}_{[n,k]} + \hat{b} \left( (x_{[n+1,k]} - x_{[n,k]} - b v_{[n,k]}) - \hat{c}_{[n,k]} \right) & n \text{ odd} \end{cases} \\ v_{[n,k]} &= \begin{cases} -\frac{1}{b} \hat{c}_{[n,k]} - r x_{[n,k]} & n \text{ even} \\ -\frac{1}{b} \hat{c}_{[n,K-k+1]} - r x_{[n,k]} & n \text{ odd} \end{cases} \end{aligned} \quad (4.21)$$

with  $k = 1, 2, \dots, K$ .

### 4.4.5 Implementation

The implementations is the same as for the observer error based controller, see section 4.3.3 for details.





## 5 Experiments

### 5.1 Laboratory Setup

The WAAM laboratory setup consists of an ABB IRB 140 Industrial Robot, a Fronius TPS 400i Welding Power Source and a Fronius WF 60i Robacta Drive CMT/w Weld Gun.

The used material is an unalloyed mild steel ER70S-6. The material composition can be seen in table 5.1. The substrate is mild steel.

Material	C	Si	Mn	Fe
%	0.08	0.9	1.45	bal.

Table 5.1: Material composition of ER70S-6.

The welding technology is Cold Metal Transfer (CMT).

The shield gas is 18 %  $\text{CO}_2$  and 82 %  $\text{Ar}$  with a flow rate of  $15 \frac{\text{l}}{\text{min}}$ .

### 5.2 Measurement of the layer heights

Measuring a height is done as follows: The welding power source applies a voltage on the wire (feed material). The weld gun is lowered onto the workpiece until the wire touches the workpiece and an electrical connection between the wire and the grounded workpiece is established. Therefore the voltage on the wire drops which triggers a digital input to stop the movement of the robot. Now, the tool centre point (TCP) of the robot is at the position of the touch disturbed by an unknown constant offset (the actual length of the wire). This means a difference of two positions can be measured since both are disturbed by same offset. For this reason, before measuring the workpiece, a reference position is measured in order to determine the offset. From then on the total height of the workpiece at certain locations can be determined.

The overall accuracy appears to be within a few  $\frac{1}{10}$  of a mm. There are systematic errors, like when the wire is pushed into the wire feeder. This occurs when the electrical connection between wire and workpiece is bad. Or when the wire is bend, which results in measuring off-centre at the desired location. Also the robots absolute accuracy plays a role (which is far worse than the repetitive accuracy). The maximum absolute error of an ABB-IRB140 is 0.8 mm and the average error is 0.35 mm according to [\*Absolute Accuracy - Industrial Robot Option 2021\*](#), an additional information pdf from the ABB website. However, we measure between two close points, therefore this maximum error will not occur.

Now, if we assume a average error (standard deviation) of 0.35 mm and want to control the layer height where the layer height reference  $\overline{\Delta z} = 1.55$  mm than we can conclude that the accuracy is not sufficient. Since, figure 5.3 suggests that the control action can only change the layer

height by about  $\pm 0.3$  mm. An error of more than the control action may lead to an unpredictable and irreproducible behaviour. A better solution for measuring the top surface position must be implemented in future projects.

## 5.3 Data Logging

In the ABB Robotware system (Operating system of the robot) was no way to conveniently log measurement data. Therefore, a TCP/IP connection between a personal computer and the robot was established. The data was then send via TCP/IP and stored in a plain text file in a certain format (one line per data set with identifier at the start).

The following data was logged:

1. timestamp
2. starting point of the wall
3. save pose for the robot
4. wire sense reference position
5.  $\overline{\Delta z}$
6.  $\overline{v}$
7.  $v_{min}$
8.  $v_{max}$
9. controller configuration (which controller)
10.  $b$
11.  $r$
12.  $\hat{b}$
13. hardware name.

## 5 Experiments

---

Also for each layer the following information was logged:

1.  $n$
2.  $z[n, k]$
3.  $x[n, k]$
4.  $\hat{c}[n, k]$  or  $\hat{x}[n, k]$  respectively
5.  $v[n, k]$

It would have been convenient to log the timestamp at starting welding, stopping welding and therefore the dwell time between layers. However, this consideration was only done after the experiments.

### 5.4 Parameter Study

The model for the control strategies according to (4.7) is

$$x[n + 1, k] = x[n, k] + b \cdot v[n, k] + c[n, k].$$

The parameter  $c$  is assumed to be unknown and slowly varying. It will be determined by online estimation. The parameter  $b$  on the other hand is assumed to be known. Therefore we have to measure or determine it beforehand. One way to do this is with equation (4.15) and one measurement  $f(\bar{v})$  at a representative travel speed  $\bar{v}$

$$b = \frac{\partial f}{\partial \bar{v}} = -\frac{f(\bar{v})}{2\bar{v}}.$$

In order to first validate equation (4.15) and on the other hand get a more robust estimation of the parameter  $b$ , several measurements at different travel speeds are taken.



Figure 5.1: Two layers for each of the 5 different tested travel speeds. One trial was redone, therefore there are six beads.

The selected travel speeds  $v^{(i)}$  are  $6 \frac{\text{mm}}{\text{s}}$ ,  $8 \frac{\text{mm}}{\text{s}}$ ,  $10 \frac{\text{mm}}{\text{s}}$ ,  $12 \frac{\text{mm}}{\text{s}}$  and  $14 \frac{\text{mm}}{\text{s}}$ .

For each travel speed two single-bead layers of approximately 10 cm in length were welded (figure 5.1). In order to get a more accurate result, the total height of the two layers was averaged to represent the height of a single layer. Further, for the evaluation of  $b$  only values in the centre are used since the data at the start and the end don't match the model.

In figure 5.2 all data points are shown. The bulk at the start and scallop at the end are clearly visible. The first 4 and last 4 data points are dropped for this reason in this evaluation. We can observe that the layer height is not dependent on the position (in the centre) therefore the data is averaged over the position  $k$  and plotted in figure 5.3 together with an

## 5 Experiments

approximation from equation (4.15) and (4.2):

$$\frac{\partial f}{\partial v} = -\frac{f(v)}{2v}$$

$$f(v) \stackrel{p=0}{=} \sqrt{\frac{A_w}{A_{wb,0}}} \cdot \sqrt{\frac{w}{v}} = C \cdot \frac{1}{\sqrt{v}}.$$

Since we know the height at  $f(v = \bar{v}) =: \bar{\Delta z}$  and the travel speed  $\bar{v}$  we can calculate the parameter  $C$  and plot the function for all other points. The expectation matches the data points very good. Also a linear approximation seems to be enough.

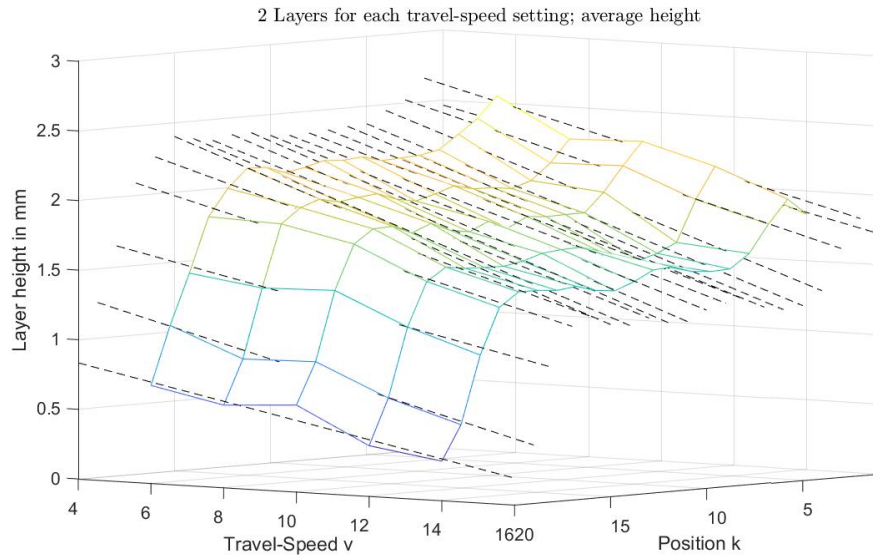


Figure 5.2: The layer height over the position for different travel speeds. The welding direction is towards positive numbers of the position  $k$ . There is a significant bulk at the start and scallop at the end. The dashed lines are linear approximations for each position. The slope of the lines is very uniform for the lines in the centre, which indicates that the model (3.5) could work well.

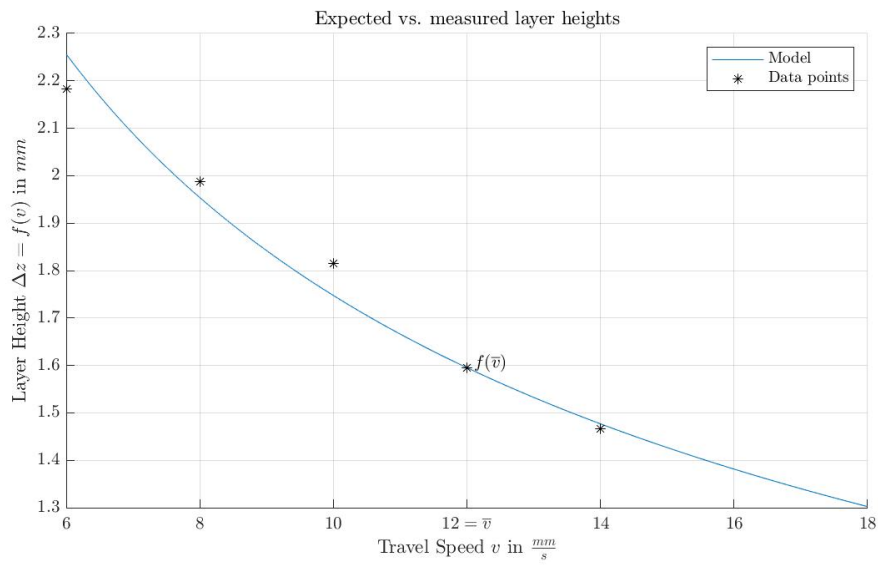


Figure 5.3: The layer heights are averaged over the weld direction around the centre for each travel speed. Also the approximation of  $f(v)$  using equation (4.15) and (4.2) is shown as the solid blue line. A good match of the model and the measurement data can be observed.

## 5.5 Unidirectional Single Bead Multi Layer Experiment

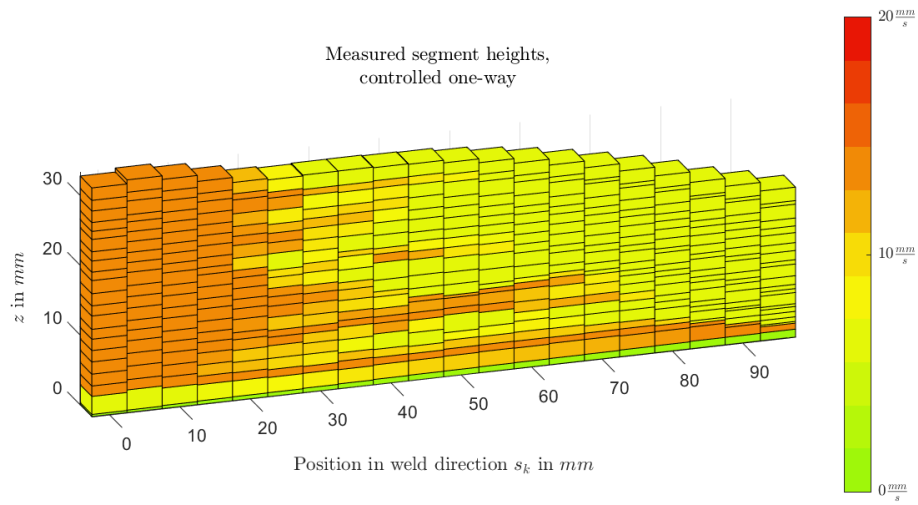


Figure 5.4: Single bead multi layer experiment with the controller from section 4.3. The cubes show the added height for each segment and layer. The colour indicates the travel speed  $v[n, k]$ .

After, validating the model (4.7) the overall system behaviour was tested. Therefore, 20 layers were welded with the controller from section 4.3. The Parameter  $b = -0.08$  was taken from the experiment in 5.4. All other parameters were chosen from short test runs of welding one or two





Figure 5.5: Result of the controlled single bead multi layer experiment. For details on the geometry see figure 5.4

layers to see how the controller behaves.

$$v_{max} = 14.0 \frac{\text{mm}}{\text{s}} \quad \dots \text{upper limit for the travel speed}$$

$$v_{min} = 6 \frac{\text{mm}}{\text{s}} \quad \dots \text{lower limit for the travel speed}$$

$$\overline{\Delta z} = 1.55 \text{ mm} \quad \dots \text{reference for the layer height}$$

$$r = -6 \quad \dots \text{controller parameter (see 4.3)}$$

$$b = -0.08 \quad \dots \text{controller parameter (see 4.3)}$$

$$\hat{b} = 0.5 \quad \dots \text{controller parameter (see 4.3)}$$

The results of the experiment can be seen in figure 5.4. It is clearly visible that there is a bulge at the start and a scallop at the end. The controller chose the travel speed to be  $v_{max}$  at the start and  $v_{min}$  at the end. From this we can conclude that it is impossible with this constraints on the control

## 5 Experiments

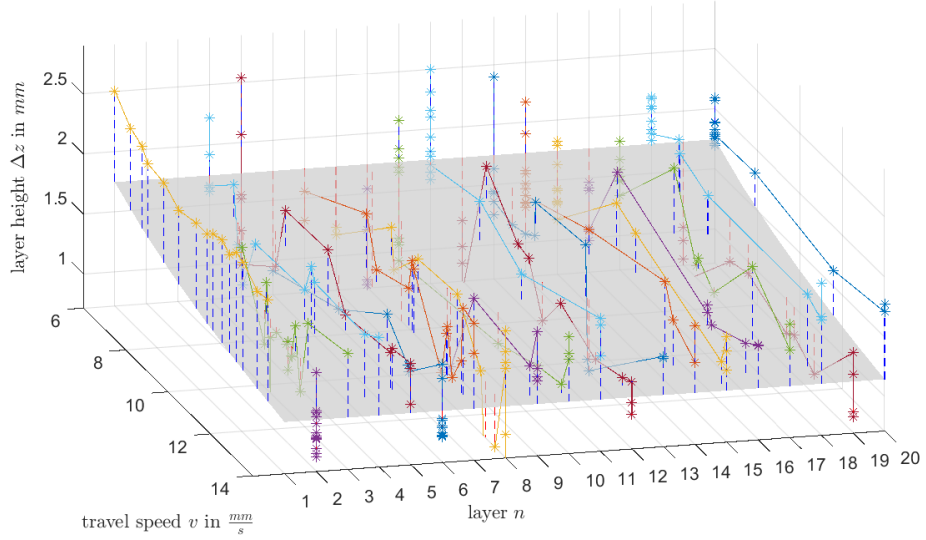


Figure 5.6: Layer height  $\Delta z$  w.r.t. the travel speed  $v$  and the layer  $n$ . Each line consists of all the measured data points (except the first and last 3 segments) for one layer. The gray surface is the model from equation (4.2). The vertical dashed lines indicate the difference to the model. Note: each point in the plot corresponds to one single measurement during the experiment. If there are multiple points at the same  $(v, n)$  location, the travel speed was measured multiple times at the same layer and yielded different results in the layer height.

value to achieve a levelled top surface. The influence from the start and stop effects is stronger than the control action.

Another effect is that the overall layer height is fading at the end. This cannot only be from the missing material at the end (see section 2.3.1) because this would only affect about the last 3 segments. We can observe that the last 10 segments are affected. The reason could be a heat accumulation towards the end of the weld bead – this will be discussed in section 5.7.

In figure 5.6 the measured layer height  $\Delta z$  w.r.t. the travel speed  $v$  and

layer  $n$  is shown. In gray the model from equation (4.2) is plotted. The first layer is higher than the model suggests. We know that the model only depends on only one constant that changes with temperature. So, if we fit the model for the first layer, it won't match the other layers well. Therefore, the model was fitted for the other layers.

The model was sufficiently good for the 2 layer experiment but does not match the data for the multi layer experiment well, even though the model should be quite robust, because it is derived from a very basic analysis. We assumed a constant cross section area and shape as well as steady state. All the material that enters a volume must eventually leave the volume. From this we got equation (3.3) which is

$$A_{wb} = A_w \cdot \frac{w}{v}$$

where  $A_{wb}$  is the cross section area of the weld bead. There are two possible sources of error. First, material leaves the volume somewhere else but  $A_{wb}$ . This was not observed during the experiments. Second, material is temporarily accumulated in the volume. This would mean averaging over the results in figure 5.6 would yield a better fit to the model. This is only partly the case. Further, if we assume a constant cross section shape for the weld bead we arrive at equation (3.5) which is

$$\Delta z = \sqrt{\frac{A_w}{A_{wb,0}}} \cdot \sqrt{\frac{w}{v}}.$$

The shape of the cross section strongly depends on the temperature field and many other influences. Also it was observed that the weld bead gets wider towards the end. This could explain the large deviations from the model. To fix this problem those influences must be stabilized. This means the temperature field must be controlled e.g. with interpass cooling.

Further, a constraint on the difference of the travel speed between two

adjacent segments should be introduced. It was observed that a rapid change in the travel speed results in a bulge at the side with the slow travel speed and a pit at the side with the fast travel speed which can also be seen in figure 5.5.

If the top surface of a segment has a small area and therefore a smaller width, the next layer will run sideways at this segment and therefore the layer height is reduced. This phenomena will be referred to as a small supporting area later on in the text. A tighter constraint on the range of the travel speed maybe helps to keep the supporting area more uniform.

### 5.5.1 Uncontrolled unidirectional single bead multi layer experiment

For comparison a 20 layer wall with the same settings but with a constant travel speed  $v = 10 \frac{\text{mm}}{\text{s}}$  was manufactured. In figure 5.7 we see that the controlled specimen is clearly more levelled on the top surface and also the effects at the start and end are less dominant. It can be concluded that the controller improves the geometrical accuracy of the process.

However, comparing the pictures of the specimens (see figure 5.5 and figure 5.8) the uncontrolled is more even at the sides. The layers appear to be constant w.r.t. the cross section shape. The controlled specimen suffers from the effect of step changes in the travel speed as discussed earlier.

## 5.5 Unidirectional Single Bead Multi Layer Experiment

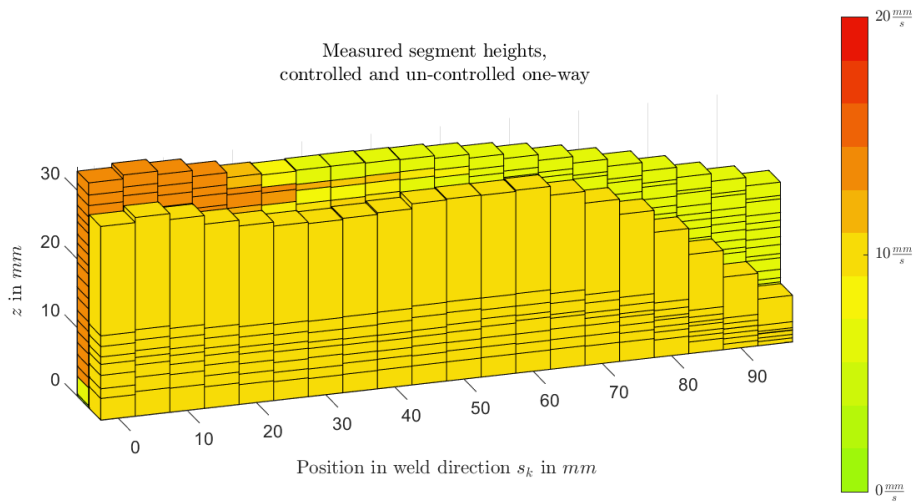


Figure 5.7: Uncontrolled single bead multi layer experiment with a constant travel speed of  $v = 10 \frac{mm}{s}$  (foreground) in comparison with the controlled single bead multi layer experiment (background). The data in the upper section was not recorded, therefore the layer borders are missing at the upper layers.

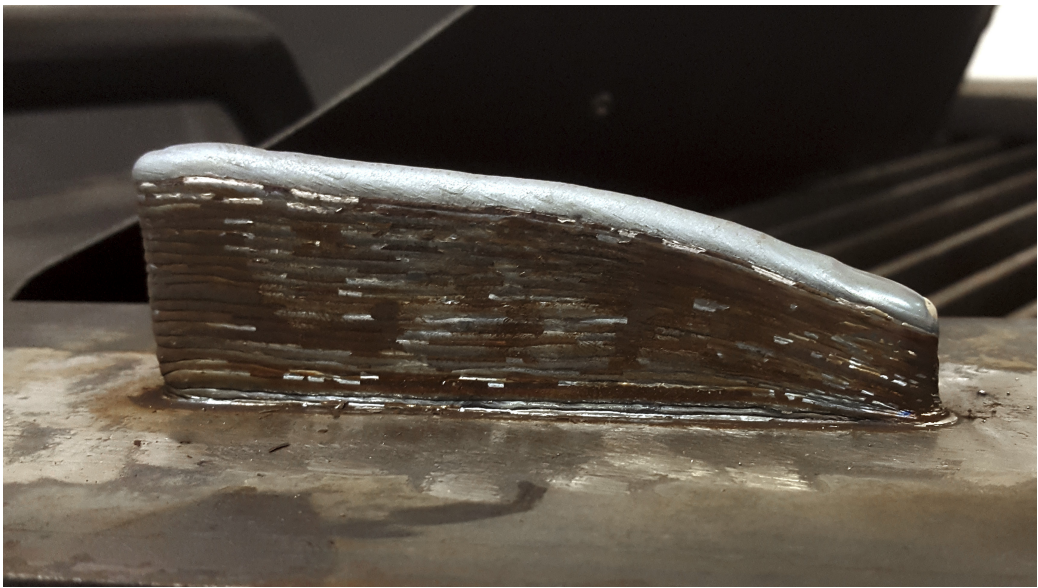


Figure 5.8: Result of the uncontrolled single bead multi layer experiment.

## 5.6 Bidirectional Single Bead Multi Layer Experiment

For the next experiment the weld direction was alternated for each layer. Which means when the first layer was welded from left to right, the second was welded from right to left. By alternating the weld direction, the effects at the start and the end partly even out which reduces the requirements on the controller.

But due to that the controller must be adapted for this operating mode. It was not possible for the state observer error based approach (section 4.3), therefore the disturbance observer based controller was used. The controller can easily be written in such a way that the alternating weld direction is taken into account. The basic control law according to equation (4.20) is

$$\begin{aligned}\hat{c}_{[n+1,k]} &= \hat{c}_{[n,k]} + \hat{b} \left( x_{[n+1,k]} - x_{[n,k]} - \hat{c}_{[n,k]} - b v_{[n,k]} \right) \\ v_{[n,k]} &= -\frac{1}{b} \hat{c}_{[n,k]} - r x_{[n,k]}.\end{aligned}$$

We postulate that the parameter  $c$  depends on the distance to the start of the bead. So the only thing that changes for the control law is that the parameter  $c$  acts on the opposite side ( $k \rightarrow K - k + 1$  for  $k = 1, 2, \dots, K$ ) for every other layer.

The resulting control law according to equation (4.21) is

$$\begin{aligned}\hat{c}_{n+1,k} &= \begin{cases} \hat{c}_{n,k} + \hat{b} ((x_{n+1,K-k+1} - x_{n,K-k+1} - b v_{n,K-k+1}) - \hat{c}_{n,k}) & n \text{ even} \\ \hat{c}_{n,k} + \hat{b} ((x_{n+1,k} - x_{n,k} - b v_{n,k}) - \hat{c}_{n,k}) & n \text{ odd} \end{cases} \\ v_{n,k} &= \begin{cases} -\frac{1}{b} \hat{c}_{n,k} - r x_{n,k} & n \text{ even} \\ -\frac{1}{b} \hat{c}_{n,K-k+1} - r x_{n,k} & n \text{ odd} \end{cases}\end{aligned}$$

## 5 Experiments

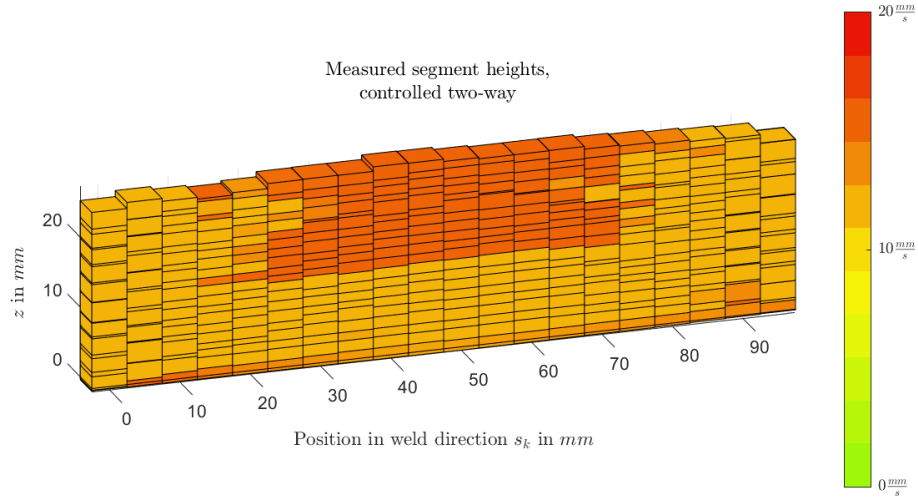


Figure 5.9: Single bead multi layer experiment with the controller from section 4.4 with alternating weld direction (equation (4.21)). The cubes show the added height for each segment and layer. The colour indicates the travel speed  $v[n, k]$ .

The controller parameters are

$$v_{max} = 16.0 \frac{\text{mm}}{\text{s}} \quad \dots \text{upper limit for the travel speed}$$

$$v_{min} = 12.0 \frac{\text{mm}}{\text{s}} \quad \dots \text{lower limit for the travel speed}$$

$$\overline{\Delta z} = 1.5 \text{ mm for } n = 1, 2, \dots, 9$$

$$\overline{\Delta z} = 1.3 \text{ mm for } n = 10, 11, \dots, 20 \quad \dots \text{reference for the layer height}$$

$$r = -6.0 \quad \dots \text{controller parameter (see 4.3)}$$

$$b = -0.08 \quad \dots \text{controller parameter (see 4.3)}$$

$$\hat{b} = 0.5 \quad \dots \text{controller parameter (see 4.3)}.$$

The result can be seen in figure 5.9. For the first 9 layers the controller was unable to meet the desired layer height of 1.5 mm. Therefore, after





Figure 5.10: Results of the controlled (middle) and uncontrolled (foreground) single bead multi layer experiment with alternating weld direction. The small wall in the background is a test run for the desired layer height  $\Delta z$ .

the 9<sup>th</sup> layer the desired layer height  $\overline{\Delta z}$  was changed to 1.3 mm. From then on, the controller was able to achieve the desired layer height but the specimen was already curved on the top surface. For this reason the control values were close to the limits for the rest of the experiment.

The top surface is much more levelled than from the unidirectional welding experiment. The effects at the start and the end were sufficiently evened out. Nevertheless, there is a slight curvature in the top surface. The controller was not able to fully level the top layer. But it was only active for 11 layers. The first and the last segment don't reach the desired height. Therefore, start and end strategies are still necessary.

It is not possible to generate a plot of  $\Delta z$  w.r.t.  $v$  and  $n$  since, there are

## 5 Experiments

mainly only 2 travel speeds per layer used  $v = 16 \frac{\text{mm}}{\text{s}}$  and  $v = 12 \frac{\text{mm}}{\text{s}}$ . Analysing those two travel speeds results in a large variance of the layer height w.r.t.  $v$  and  $n$ . Thus, the stabilization of the temperature field as well as the constraint on the change of the control value is still necessary.

### 5.6.1 Uncontrolled bidirectional single bead multi layer experiment

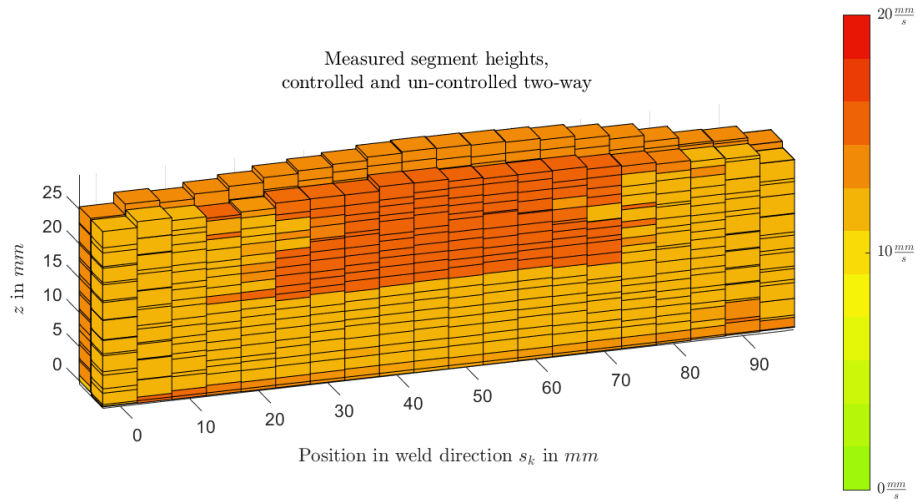


Figure 5.11: Uncontrolled bidirectional single bead multi layer experiment with a constant travel speed of  $v = 14 \frac{\text{mm}}{\text{s}}$  (background) in comparison with the controlled bidirectional single bead multi layer experiment (foreground).

For this method as well a uncontrolled comparison specimen also with 20 layers was manufactured. The constant travel speed is  $v = 14 \frac{\text{mm}}{\text{s}}$ . The results of both experiments can be seen in figure 5.11. The controlled specimen is more levelled at the top surface.

From the comparison it can be concluded that the controller improves the geometrical accuracy of the process.

If we take a closer look at the edges a strange behaviour can be seen. The controlled specimen was welded with a travel speed of  $v = 12 \frac{\text{mm}}{\text{s}}$  and the uncontrolled with  $v = 14 \frac{\text{mm}}{\text{s}}$  but the two specimen match height at the edges. The average layer height seems to be independent of the travel speed in this areas in some extent.

### 5.7 Temperature Field during the welding process

In order to analyse the temperature field during the welding process a specimen was prepared with thermocouples at specific locations. The specimen had the shape of a thin wall (see figure 5.12). Additionally, the temperature of the middle segment was measured by an infrared temperature sensor.

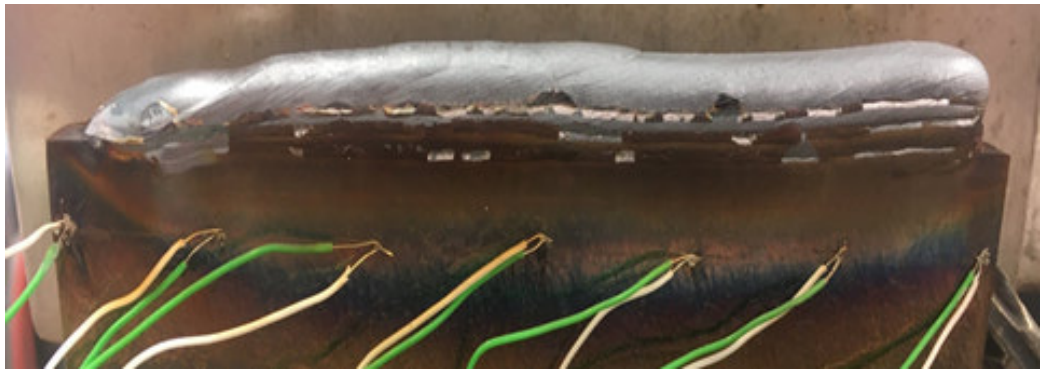


Figure 5.12: Preparation of the specimen for the temperature field experiment.

The experiment consists of two measured passes. For the first pass (layer 1), the specimen was at room temperature. For the second pass (layer 4), the specimen was at 100°C heated by a heat plate. The raw data i.e. the temperature w.r.t. time and weld length position is plotted in figure 5.13.

For the model derivation in chapter 3 equation (3.5) a non-changing cross section shape of the weld bead was required and therefore a non-changing temperature field around the weld pool. In other words, the temperature field must be quasi static. A quasi static temperature field in this context means that the field doesn't depend on time. Of course in global coordinates the temperature field is depending on time because

## 5.7 Temperature Field during the welding process

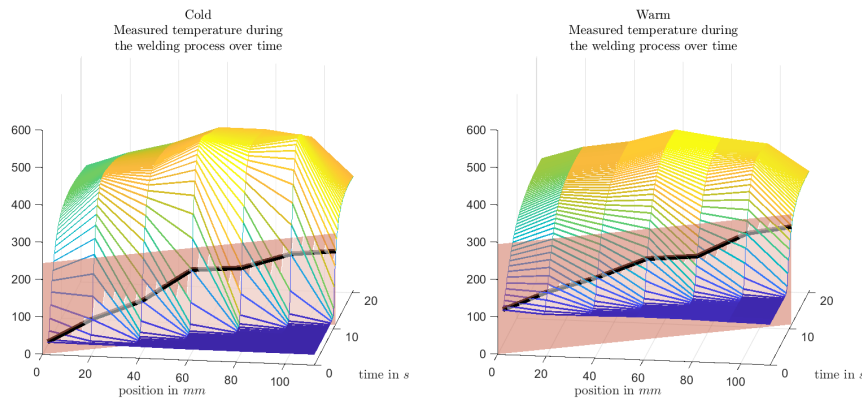


Figure 5.13: Temperature over time for both passes of the temperature field experiment. The red surface is the position of the weld gun over time. The black curve is the temperature below the weld gun. The data is also shown as a 2D-plot in figure 5.14.

of the moving heat source. But if we change perspective and look at the problem from the weld gun coordinate frame, a quasi static temperature field will eventually be reached.

However, if we look at figure 5.13 we can observe from the black curve (the temperature below the weld gun) that the temperature field is depending on time. It can be seen more clearly if the curve is plotted explicitly, this is done in figure 5.14. There, it can be observed that the temperature below the weld gun rises about  $138^{\circ}\text{C}$  over the length of the specimen if the base plate is heated and it rises about  $169^{\circ}\text{C}$  if the base plate is cold. Note, that for the experiment with the heated base plate the distance to the weld gun is higher (3 layers higher).

It is well known that this temperature increase will eventually reach a saturation. So, how is it possible to get those results? Let's consider the infinitely extended cold workpiece before the arc was ignited. The

## 5 Experiments

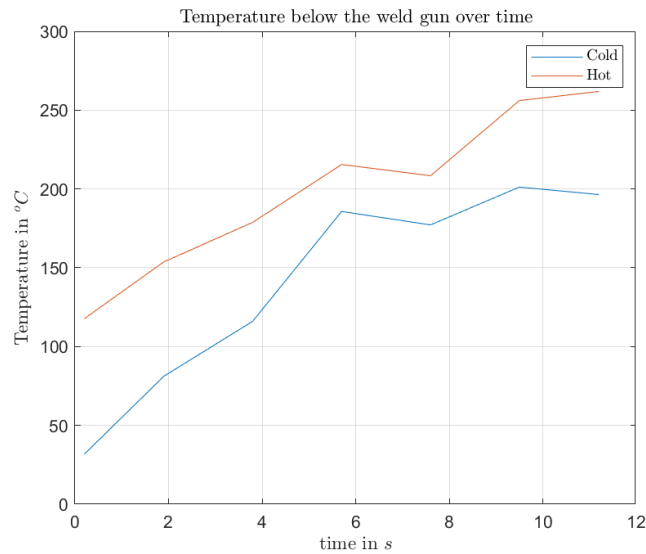


Figure 5.14: Temperature below the weld gun over the length of the specimen. Keep in mind that the measurements were not taken at the same instance of time but only when the weld gun was above the measurement point.

temperature is constant at every point. Then we ignite the arc i.e. the heat source. At this exact moment the temperature is still constant everywhere except at the exact location of the heat source. After some time a quasi stationary temperature field w.r.t. the weld gun coordinate frame will eventually be reached. But during the time between the ignition of the arc and the quasi stationary field the temperature field has to evolve from an initial field to what the quasi stationary field looks like. And this is exactly what we see in the data.

Let's plot the data again but in the weld gun coordinate frame. This is done in figure 5.15. If the temperature field was quasi-static the plotted data would be constant along the time axis. However, in the upper right corner of the left plot in figure 5.15 it looks like the temperature field stops

## 5.7 Temperature Field during the welding process

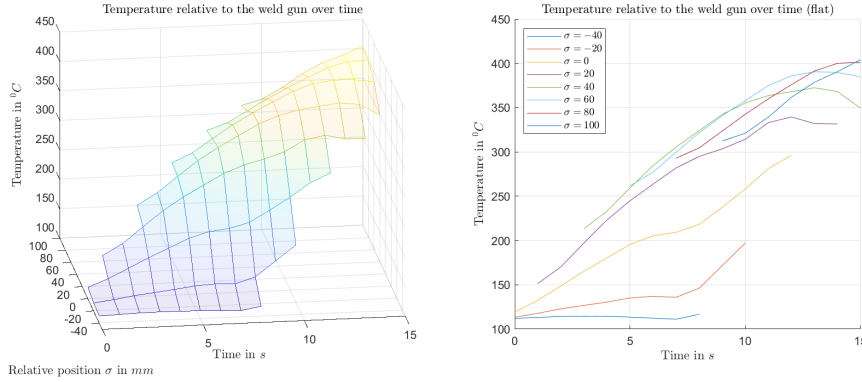


Figure 5.15: Temperature relative to the weld pool. A relative position  $\sigma = 20$  mm means that the temperature 20 mm behind (i.e. were the weld gun was 2 s ago) the weld gun is shown. The data was interpolated and implicitly smoothed in order to generate a non-distorted mesh-grid. A mesh-grid line parallel to the time-temperature plane is the temperature development of a point  $\sigma$  behind the weld gun. The data from the second pass (preheated baseplate, layer 4) was used.

rising and becomes quasi stationary.

The conclusion from this experiment is, that the transition to the quasi stationary field can not be neglected for such a short weld. In this experiment it lasts at least 10 s to build up the quasi static temperature field. During this transition the temperature somewhere below the weld gun rises about 169 °C for the cold base plate and about 138 °C for the heated base plate. Therefore, we can assume that the weld pool dimensions will increase.

This further means the assumptions for equation (3.5) are not met and therefore the equation is not accurate. However, if this transition is the same for each layer the controllers proposed in this thesis could still be used because of the adaptive nature of the controller. This could possibly

## 5 Experiments

---

be achieved by introducing interpass cooling.



## 6 Conclusion

### 6.1 Review of the Content

In chapter 1 a review of the current state of the art is given. It is discussed what Wire Arc Additive Manufacturing (WAAM) is, what the aim for this technology is, what advantages there are w.r.t. to conventional methods and the drawbacks.

In chapter 2 the different welding technologies in WAAM are explained in detail, the commonly used materials and there challenges, a detailed review of the overall challenges in WAAM among them, geometrical challenges and how to deal with those e.g. using ancillary processes.

In chapter 3 the signifiant quantities for the process are listed, explained and also their relations are discussed. Also the focus of this work i.e. the laboratory setup, the measured and controlled quantities and limitations are discussed. The Problem statement is given and the consequences for the modelling and control: A novel modelling approach is presented where, in contrast to the literature, the layer height does not need to be measured continuously.

In chapter 4 the modelling approach is formulated and derived. Two controllers are proposed and derived. Also their stability and the implementation as well as limitations are discussed.

In chapter 5 the experiments are presented and discussed.

## 6.2 Discussion of the results

### 6.2.1 Layer Height w.r.t. travel speed

In chapter 3 in equation (3.5) the relation between the layer height  $\Delta z$  and the ratio of wire feed speed and travel speed  $\frac{w}{v}$  is derived for the assumption of a constant cross section shape of the weld bead. Also, Adebayo, 2013 found that keeping this ratio constant results in a constant cross section.

$$\Delta z = \sqrt{\frac{A_w}{A_{wb,0}}} \cdot \sqrt{\frac{w}{v}}$$

The equation is also derived for the assumption of an delay in the control action w.r.t. the layer height in chapter 4, see equation (4.2)

$$\Delta z [n + 1, k] = \sqrt{\frac{A_w}{A_{wb,0}}} \cdot \sqrt{p \frac{w [n, k - 1]}{v [n, k - 1]} + (1 - p) \frac{w [n, k]}{v [n, k]}}.$$

In the experiment in chapter 5.4 the model is validated. The result is a good match of the experiment and the measured data. Nevertheless, the experiment was done only for 2 layers. From the experiments in chapter 5.5 we know that for higher layers the layer height varies heavily. Possible reasons can be the changing supporting area (as discussed in chapter 5.5)

of the layer underneath, rapid changes in the travel speed and the changing temperature field around the weld pool. To further investigate into this problem the experiment in chapter 5.7 was conducted. The results show that over the length of the specimen the temperature below the weld pool is increasing. From this it can be concluded that the temperature field is not quasi-static w.r.t. the weld pool but transient. The results show an increase of around 150°C over the length of the specimen.

In order to apply the model from equation 3.5 we need a constant temperature field around the weld pool. Therefore, ancillary processes must be implemented to achieve this goal. One technique that possibly reduces the change in the temperature field is inter pass cooling. There will still be an increase in temperature over the length of the workpiece but it will be a predictable increase. This fits into the model from equation 4.7

$$x[n + 1, k] = x[n, k] + b \cdot v[n, k] + c[n, k]$$

where the constant  $c$  will be estimated by the observer even with a changing temperature field as long as the evolution of the temperature field stays the same for each pass.

Another technique would be the preheating of the surface in front of the weld pool. Thus, the temperature field is controlled directly. Even better results can be achieved by actively cooling the workpiece like Li et al., 2018 suggests.

Another influence on the cross section shape of the weld bead is the supporting area of the underlying layer as discussed in chapter 5.5. If the width and therefore the top surface area of a segment is small, the next layer will run sideways at this segment – thus the shape of the weld bead is changed. The reason for a changing bead width in the first place could be heat accumulation as discussed earlier or big changes in the travel speed.

In the experiments in chapter 5.5 we can observe that a rapid change in the travel speed results in a bulge at one side and a pit on the other side of the rapid change. Therefore the bead width is non-uniform. A constraint on the change of the travel speed between adjacent segments can be added to counteract this behaviour. However, the suggested control law in this thesis does not support constraints on the change of a quantity. It would be necessary to derive a new controller, e.g. a Model Predictive Controller (MPC). The drawback of an MPC is that it likely cannot be implemented directly in the ABB Robot. To be mentioned, if we eliminate the change of the temperature field around the weld pool the underlying supporting area will also become more uniform which relaxes the constraints on the change of the travel speed between adjacent segments.

### 6.2.2 Heat input

In chapter 3 in equation (3.6) the volumetric heat input is discussed.

$$H_V = \frac{\eta}{A_w} \cdot \frac{I_w \cdot U_{arc}}{w}$$

If this quantity is constant also the temperature field around the weld pool should more or less be quasi-static after an initial transient period. This is yet to be verified. However, from this relation we can derive a constraint on the wire feed speed or the arc power in order to keep the temperature field quasi-static which would further help to fulfil the requirements for equation (3.5) to hold.

### 6.2.3 Delay in $\frac{w}{v}$

In chapter 4 in equation (4.2)

$$\Delta z[n+1, k] = \sqrt{\frac{A_w}{A_{wb,0}}} \cdot \sqrt{p \frac{w[n, k-1]}{v[n, k-1]} + (1-p) \frac{w[n, k]}{v[n, k]}}$$

a delay of the control action w.r.t  $\frac{w}{v}$  is introduced. This is based on the findings of Xiong and G. Zhang, 2014 as well as Doumanidis and Kwak, 2002. A change in the wire feed speed or the travel speed does not take effect immediately but is delayed due to the finite dimensions of the weld pool. One question is still open: is the delay constant? If we move very slow with a very small heat input, the weld pool is small and therefore the delay. If we move fast with a high heat input, the weld pool is longer and therefore the delay higher. Can we still assume a constant delay? This remains to be verified.

The controllers in chapter 4 can be derived with this delay as well because the quantity  $v[k-1, n]$  is known before the evaluation of  $v[k, n]$ . The improvements on the geometrical accuracy with this approach have to be tested as well.

## 6.3 Discussion of the Controllers

From the experiments in chapter 5.5 we can conclude that the controller improves the geometrical accuracy, although the model from equation (4.2) is not suited, due to the changing temperature field. Nevertheless, the heat accumulation makes it impossible for any controller to achieve a levelled surface with the given constraints – see figure 5.4. In order to

reach the control goal (levelled top surface), the temperature field has to be controlled.

The experiments in chapter 5.6 delivered a useful result. It was shown that by alternating the weld direction the top surface was levelled with only a few mm difference in height over the length. The result is that the controller – despite the problems with the model – improves the geometrical accuracy. To further improve the results without any changes in the hardware, a constant dwell time should be introduced as well as a parameter study to find the best suited set of parameters for the controller.

To further improve the controller in chapter 5.6 the findings discussed in chapter 6.2.1 should be applied i.e. a quasi-static temperature field w.r.t. weld pool. This would also fulfil the prerequisites for the use of the model from equation (4.2).

## 7 Outlook

There is still work to do in order to improve the geometrical accuracy of the GMAW (or more specific the CMT) process to a degree that also non-thin-wall structures can be manufactured with the approach presented in this thesis.

First, let's focus on the setup. At the moment, the only measurement quantity is the total height. This quantity is measured through contact based determination of the robots TCP from which the layer height is derived. This is not a accurate approach. Therefore, the measurement of the geometry should be improved and extended with e.g. laser profilometry (see figure 7.1). With this technique the layer height as well as the layer width can be measured continuously or after each pass. The layer width can be useful not only to estimate the cross section area but also to estimate the heat input to verify the model.

Further, we need more measurements. Beside the geometry we need the wire feed speed, the arc voltage, the welding current and the interpass temperature. Wire feed speed, arc voltage and current should be supplied by the welding power source. The interpass temperature can be measured using a IR temperature sensor. Having this measurements, the experiments are repeatable and the results can be interpreted with more certainty.

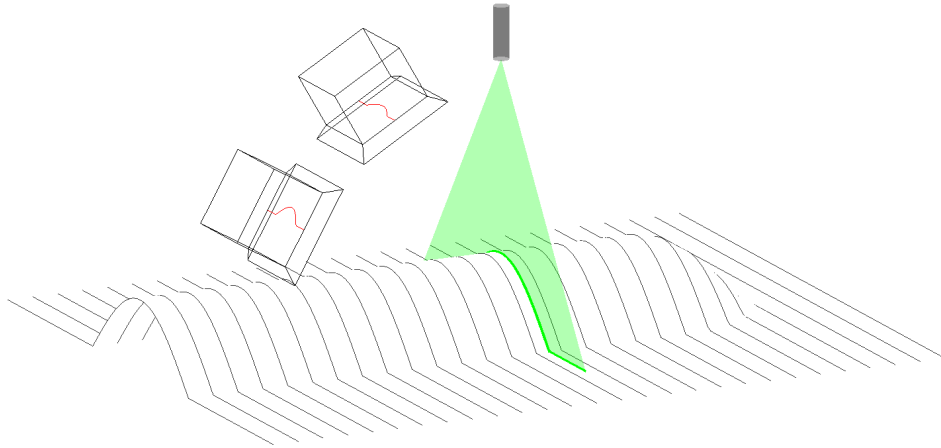


Figure 7.1: Laser profilometry. The laser stripe is projected onto the intersection of the surface of the weld bead and the plane (let's define it as the  $xz$ -plane) in which the laser is. The camera is tilted by an angle  $\alpha$  w.r.t. the  $z$  axis. Now, the camera sees a projection of the laser stripe into the image plane. With the fact that the laser strip can only be in the  $xz$ -plane the true  $xyz$ -coordinates can be determined. Two cameras are shown to emphasize the dependency of the resolution on the angle  $\alpha$ .

Second, we need more control of the process. It was shown in the experiments in chapter 5.5 and chapter 5.6 that the lack of a quasi stationary temperature field makes the control of the bead geometry impossible or hardly possible (in case of the alternating weld direction). The temperature field should be controllable. This can be done e.g. by adjusting the heat input i.e. by adjusting the wire feed speed. Another solution can be interpass cooling or heating. One approach could be to heat the surface in front of the weld pool in order to achieve the desired temperature field e.g. with an additional GTAW torch.



---

Third, the model should be verified for the new setup – equation (4.2) as well as equation (3.6)

$$\Delta z[n+1, k] = \sqrt{\frac{A_w}{A_{wb,0}}} \cdot \sqrt{p \frac{w[n, k-1]}{v[n, k-1]} + (1-p) \frac{w[n, k]}{v[n, k]}}$$

$$H_V = \eta \cdot \frac{P_{arc}}{v A_{wb}}$$

and therefore equation 4.7

$$x[n+1, k] = x[n, k] + b \cdot v[n, k] + c[n, k].$$

If the model works fine the proposed controllers can be used.



# Bibliography

- Absolute Accuracy - Industrial Robot Option* (Oct. 13, 2021). URL: [https://library.e.abb.com/public/0f879113235a0e1dc1257b130056d133/Absolute%20Accuracy%20EN\\_R4%20US%2002\\_05.pdf](https://library.e.abb.com/public/0f879113235a0e1dc1257b130056d133/Absolute%20Accuracy%20EN_R4%20US%2002_05.pdf) (cit. on p. 40).
- Adebayo, Adeyinka (2013). "Characterisation of integrated WAAM and machining processes". In: (cit. on pp. 9, 11, 18, 64).
- Barrionuevo, Germán Omar et al. (May 2021). "Comparative Evaluation of Machine Learning Regressors for the Layer Geometry Prediction in Wire arc Additive manufacturing". In: *2021 IEEE 12th International Conference on Mechanical and Intelligent Manufacturing Technologies (ICMIMT)*, pp. 186–190. DOI: [10.1109/ICMIMT52186.2021.9476168](https://doi.org/10.1109/ICMIMT52186.2021.9476168).
- Colegrove, Paul and Stewart Williams (2013). "High deposition rate high quality metal additive manufacture using wire + arc technology". In: *Cranfield University* (cit. on p. 2).
- Cunningham, C.R. et al. (2018). "Invited review article: Strategies and processes for high quality wire arc additive manufacturing". In: *Additive Manufacturing* 22, pp. 672–686. ISSN: 2214-8604. DOI: <https://doi.org/10.1016/j.addma.2018.06.020>. URL: <https://www.sciencedirect.com/science/article/pii/S2214860418303920> (cit. on pp. 13–15).
- Dass, Adrita and Atieh Moridi (2019). "State of the art in directed energy deposition: From additive manufacturing to materials design". In: *Coatings* 9.7, p. 418 (cit. on pp. 1, 5).

- Derekar, K. S. (2018). "A review of wire arc additive manufacturing and advances in wire arc additive manufacturing of aluminium". In: *Materials Science and Technology* 34.8, pp. 895–916. DOI: [10.1080/02670836.2018.1455012](https://doi.org/10.1080/02670836.2018.1455012). eprint: <https://doi.org/10.1080/02670836.2018.1455012>. URL: <https://doi.org/10.1080/02670836.2018.1455012> (cit. on pp. 6, 8, 10, 11).
- Dhinakaran, V. et al. (2020). "Wire Arc Additive Manufacturing (WAAM) process of nickel based superalloys – A review". In: *Materials Today: Proceedings* 21. International Conference on Recent Trends in Nanomaterials for Energy, Environmental and Engineering Applications, pp. 920–925. ISSN: 2214-7853. DOI: <https://doi.org/10.1016/j.matpr.2019.08.159>. URL: <https://www.sciencedirect.com/science/article/pii/S2214785319331463> (cit. on p. 8).
- Ding, Donghong et al. (2015). "A multi-bead overlapping model for robotic wire and arc additive manufacturing (WAAM)". In: *Robotics and Computer-Integrated Manufacturing* 31, pp. 101–110. ISSN: 0736-5845. DOI: <https://doi.org/10.1016/j.rcim.2014.08.008>. URL: <https://www.sciencedirect.com/science/article/pii/S0736584514000696>.
- Dinovitzer, Malcolm et al. (2019). "Effect of wire and arc additive manufacturing (WAAM) process parameters on bead geometry and microstructure". In: *Additive Manufacturing* 26, pp. 138–146. ISSN: 2214-8604. DOI: <https://doi.org/10.1016/j.addma.2018.12.013>. URL: <https://www.sciencedirect.com/science/article/pii/S2214860418306286> (cit. on p. 3).
- Doumanidis, Charalabos and Yong-Min Kwak (2002). "Multivariable adaptive control of the bead profile geometry in gas metal arc welding with thermal scanning". In: *International Journal of Pressure Vessels and Piping* 79.4, pp. 251–262. ISSN: 0308-0161. DOI: [https://doi.org/10.1016/S0308-0161\(02\)00024-8](https://doi.org/10.1016/S0308-0161(02)00024-8). URL: <https://www.sciencedirect.com/science/article/pii/S0308016102000248> (cit. on pp. 9, 24, 26, 67).
- Horn, Martin (2019). *Lecture notes in Prozessautomatisierung* (cit. on p. 33).

- Joseph, Andrew Paul (2001). "Assessing the effects of GMAW-pulse parameters on arc power and weld heat input". PhD thesis. The Ohio State University (cit. on p. 21).
- Li, Fang et al. (2018). "Thermoelectric Cooling-Aided Bead Geometry Regulation in Wire and Arc-Based Additive Manufacturing of Thin-Walled Structures". In: *Applied Sciences* 8.2. ISSN: 2076-3417. DOI: [10.3390/app8020207](https://doi.org/10.3390/app8020207). URL: <https://www.mdpi.com/2076-3417/8/2/207> (cit. on pp. 10, 13, 65).
- Liberini, Mariacira et al. (2017). "Selection of Optimal Process Parameters for Wire Arc Additive Manufacturing". In: *Procedia CIRP* 62. 10th CIRP Conference on Intelligent Computation in Manufacturing Engineering - CIRP ICME '16. [Edited by: Roberto Teti, Manager Editor: Doriana M. D'Addona], pp. 470–474. ISSN: 2212-8271. DOI: <https://doi.org/10.1016/j.procir.2016.06.124>. URL: <https://www.sciencedirect.com/science/article/pii/S2212827117301968>.
- Singh, Sagar, Satish kumar Sharma, and Dinesh W. Rathod (2021). "A review on process planning strategies and challenges of WAAM". In: *Materials Today: Proceedings*. ISSN: 2214-7853. DOI: <https://doi.org/10.1016/j.matpr.2021.02.632>. URL: <https://www.sciencedirect.com/science/article/pii/S2214785321017831> (cit. on p. 17).
- Williams, S. W. et al. (2016). "Wire + Arc Additive Manufacturing". In: *Materials Science and Technology* 32.7, pp. 641–647. DOI: [10.1179/1743284715Y.0000000073](https://doi.org/10.1179/1743284715Y.0000000073). eprint: <https://doi.org/10.1179/1743284715Y.0000000073>. URL: <https://doi.org/10.1179/1743284715Y.0000000073> (cit. on pp. 1, 3, 6, 7, 11).
- Wu, Binta, Donghong Ding, et al. (2017). "Effects of heat accumulation on the arc characteristics and metal transfer behavior in Wire Arc Additive Manufacturing of Ti6Al4V". In: *Journal of Materials Processing Technology* 250, pp. 304–312. ISSN: 0924-0136. DOI: <https://doi.org/10.1016/j.jmatprotec.2017.07.037>. URL: <https://www.sciencedirect.com/science/article/pii/S0924013617303370> (cit. on pp. 3, 7, 14).

- Wu, Bintaoy, Zengxi Pan, et al. (2018). "A review of the wire arc additive manufacturing of metals: properties, defects and quality improvement". In: *Journal of Manufacturing Processes* 35, pp. 127–139. ISSN: 1526-6125. DOI: <https://doi.org/10.1016/j.jmapro.2018.08.001>. URL: <https://www.sciencedirect.com/science/article/pii/S1526612518310739> (cit. on pp. 1–3, 6, 8, 11–13).
- Xiong, Jun, Ziqiu Yin, and Weihua Zhang (2016). "Closed-loop control of variable layer width for thin-walled parts in wire and arc additive manufacturing". In: *Journal of Materials Processing Technology* 233, pp. 100–106. ISSN: 0924-0136. DOI: <https://doi.org/10.1016/j.jmatprotec.2016.02.021>. URL: <https://www.sciencedirect.com/science/article/pii/S0924013616300516> (cit. on pp. 9, 24).
- Xiong, Jun and Guangjun Zhang (2014). "Adaptive control of deposited height in GMAW-based layer additive manufacturing". In: *Journal of Materials Processing Technology* 214.4, pp. 962–968. ISSN: 0924-0136. DOI: <https://doi.org/10.1016/j.jmatprotec.2013.11.014>. URL: <https://www.sciencedirect.com/science/article/pii/S0924013613003415> (cit. on pp. 24, 26, 67).